FREE INFLATION OF AN ANISOTROPIC HYPERELASTIC CIRCULAR MEMBRANE

A Thesis Submitted
In Partial Fulfilment of the Requirements for the Degree of

MASTER OF TECHNOLOGY

in

MECHANICAL ENGINEERING(CAAD)

By

Sunil Bishwakarma
(Roll No. 24/CAD/10)

Under the Supervision of

Dr. Satyajit Sahu
Assistant Professor
Department of Mechanical Engineering
Delhi Technological University

Department of Mechanical Engineering

DELHI TECHNOLOGICAL UNIVERSITY
(Formerly Delhi College of Engineering)
Shahbad Daulatpur, Main Bawana Road, Delhi-110042, India

June, 2026

DELHI TECHNOLOGICAL UNIVERSITY

(Formerly Delhi College of Engineering)

Shahbad Daulatpur, Main Bawana Road, Delhi-110042

CANDIDATE'S DECLARATION

I, **SUNIL BISHWAKARMA** (Roll No. 24/CAD/10), hereby certify that the work which is being presented in the thesis entitled **"Free Inflation of an Anisotropic Hyperelastic Circular Membrane"** in partial fulfilment of the requirements for the award of the Degree of **Master of Technology**, submitted in the **Department of Mechanical Engineering**, Delhi Technological University, is an authentic record of my own work carried out during the period from **January 2026** to **June 2026** under the supervision of **Dr. Satyajit Sahu**.

The matter presented in the thesis has not been submitted by me for the award of any other degree of this or any other Institute.

Candidate's Signature

This is to certify that the student has incorporated all the corrections suggested by the examiners in the thesis and the statement made by the candidate is correct to the best of our knowledge.

Signature of Supervisor **Signature of External Examiner**

DELHI TECHNOLOGICAL UNIVERSITY

(Formerly Delhi College of Engineering)

Shahbad Daulatpur, Main Bawana Road, Delhi-110042

CERTIFICATE BY THE SUPERVISOR(s)

Certified that **SUNIL BISHWAKARMA** (Roll No. 24/CAD/10) has carried out their research work presented in this thesis entitled **"Free Inflation of an Anisotropic Hyperelastic Circular Membrane "** for the award of **Master of Technology** from Department of Mechanical Engineering, Delhi Technological University, Delhi, under my supervision. The thesis embodies results of original work, and studies are carried out by the student himself/herself, and the contents of the thesis do not form the basis for the award of any other degree to the candidate or to anybody else from this or any other University/Institution.

Signature

Dr. Satyajit Sahu

Assistant Professor

Department of Mechanical Engineering

Delhi Technological University, Delhi-110042

Date: _____________

DELHI TECHNOLOGICAL UNIVERSITY

(Formerly Delhi College of Engineering)

Shahbad Daulatpur, Main Bawana Road, Delhi-42

PLAGIARISM VERIFICATION

Title of the Thesis:____

____

Total Pages: __________ Name of the Scholar __________________________________

Supervisor(s):

(1) _________________________

(2) _________________________

(3) _________________________

Department: ____

This is to report that the above thesis was scanned for similarity detection. Process and outcome is given below:

Software used: _________ Similarity Index: ________ Total Word Count: ___________

Date: ________________________

Candidate's Signature

Signature of Supervisor(s)

DELHI TECHNOLOGICAL UNIVERSITY

(Formerly Delhi College of Engineering)

Shahbad Daulatpur, Main Bawana Road, Delhi-42

CERTIFICATE OF THESIS SUBMISSION FOR EVALUATION

(Submit in Duplicate)

1. Name: ....
2. Roll No.: ....
3. Thesis title: ....

   ……………………………………………………………………………………...
4. Degree for which the thesis is submitted: ....
5. Faculty of the University to which the thesis is submitted:

   ....
6. Thesis Preparation Guide was referred to for preparing the thesis. YES ☐ NO ☐
7. Specifications regarding thesis format have been closely followed. YES ☐ NO ☐
8. The contents of the thesis have been organized based on the guidelines.

   YES ☐NO ☐
9. The thesis has been prepared without resorting to plagiarism. YES ☐ NO ☐
10. All sources used have been cited appropriately. YES ☐ NO ☐
11. The thesis has not been submitted elsewhere for a degree. YES ☐ NO ☐
12. Submitted 2 spiral bound copies plus one CD. YES ☐ NO ☐

(Signature of Candidate)

Name(s): ....

Roll No.: ....

DELHI TECHNOLOGICAL UNIVERSITY

(Formerly Delhi College of Engineering)

Shahbad Daulatpur, Main Bawana Road, Delhi-42

CERTIFICATE OF FINAL THESIS SUBMISSION

(To be submitted in duplicate)

1. Name: ....
2. Roll No: ....
3. Thesis title: ....
   …………………………………………………………………………………
4. Degree for which the thesis is submitted: ....
5. Faculty (of the University to which the thesis is submitted)
   ....
6. Thesis Preparation Guide was referred to for preparing the thesis. YES ☐ NO ☐
7. Specifications regarding thesis format have been closely followed. YES ☐ NO ☐
8. The contents of the thesis have been organized based on the guidelines. YES ☐ NO ☐
9. The thesis has been prepared without resorting to plagiarism. YES ☐ NO ☐
10. All sources used have been cited appropriately. YES ☐ NO ☐
11. The thesis has not been submitted elsewhere for a degree. YES ☐ NO ☐
12. All the correction has been incorporated. YES ☐ NO ☐
13. Submitted 2 hard bound copies plus one CD. YES ☐ NO ☐

(Signature(s) of the Supervisor(s)) (Signature of Candidates)

Name(s): Dr. Satyajit Sahu

Name: Sunil Bishwakarma

Roll No: 24/CAD/10

ABSTRACT

Inflation of a thin elastic membrane is a well-studied classical problem in nonlinear continuum mechanics; however, the impact of material anisotropy on the inflation response of hyperelastic materials has yet to be thoroughly researched. Therefore, this research examines the axisymmetric axial deformation behaviour of a circular membrane composed of an incompressible anisotropic Mooney-Rivlin material being blown up against a uniform transverse pressure load, without any initial radial pre-strain.

The derivation of governing equations comes from the principle of stationary potential energy, with the strain energy density function being expressed using the two principal stretches from the plane of the membrane and an anisotropic invariant $I_4 = \lambda_1^2$ for the thickness of the membrane. The invariant thus gives rise to one stretch in the thickness direction, since there can be no volume change under the assumption of incompressibility. Each of these principal stretches is identified by introducing the appropriate field variable so that the governing equations are reduced from two second-order ordinary differential equations into a system of three first-order ordinary differential equations. The converting or changing of the governing equations into a different format allows for easier numerical integration using standard initial value-problem solvers.

The two-point boundary value problem resulting from this research has been solved using the combination of the shooting method and the optimization procedure using fminsearch. The primary advancement in the numerical solution is the established verification of the scaling invariance property inherent to the equilibrium equations applies to the anisotropic equations, thus allowing for the elimination of the arc-length continuation methods in all cases where the pressure-stretch relationship has limit point instability.

Presented here are numerical results for two different pairs of Mooney-Rivlin material parameters, $\alpha = \frac{C_2}{C_1} = 0.01, 0.03, 0.1$ and four different levels of anisotropy, $\zeta = 0, 0.01, 0.03, 0.05$, with no pre-stretch ($\beta = 1$). The results show that anisotropy causes a stiffening effect in the inflation response, through the pressure-deflection curves. The pressure-deflection curves for $\alpha = 0.01$ (close to Neo-Hookean behaviour) show that the limit point is always there regardless of connectivity level ζ. Critical pressures remain about the same for each value of ζ. When working with $\alpha = 0.1$ (which has a large component for C_2), the response is monotonic and stable; but as the value of ζ increases, maximum deflections will decrease by as much as 56 at a pressure of 10.

The stress resultants show that inflation creates anisotropic behaviour in the meridional and circumferential components of the material properties (highest stresses at the clamped edges). The peak stress at the clamp reduces and circumferential stress increases at the interior of the structure when the anisotropy parameter is increased.

The 3D surface reconstruction and membrane profiles have shown that hysteresis in the anisotropic membrane is less than that of the isotropic membrane at similar elevations (pressure). This study will benefit the designer of any inflatable structure requiring uniform strains and controlled directional stiffness.

Keywords - Anisotropic membrane; Mooney-Rivlin Material; Finite Membrane; Circular Membrane; Anisotropic Parameter; Strain Energy Function; Shooting Method; Scaling.

ACKNOWLEDGEMENTS

The completion of this research would not have been possible without the consistent support and guidance of many individuals and institutions.

First and foremost, I express my deepest gratitude to my thesis supervisor, **Dr. Satyajit Sahu**, Assistant Professor in the Department of Mechanical Engineering at Delhi Technological University. His profound understanding of continuum mechanics, coupled with his patience in guiding a novice researcher, has been the cornerstone of this work. He taught me that nonlinear problems are not obstacles but opportunities to think differently.

I am thankful to the **Delhi Technological University** for providing the computational facilities and library resources that enabled this research. The university's commitment to fostering research in emerging areas of mechanical engineering is truly commendable.

I would also like to express gratitude toward **Prof. B.B Arora** (Head of Department, Mechanical Engineering, DTU) for extending his support and guidance

My sincere thanks go to the **Department of Mechanical Engineering** faculty members, especially, **Dr. Atul Kumar Agrawal** whose periodic reviews and constructive criticisms helped refine the direction of this work.

I acknowledge with gratitude the financial support provided by the **Indian Council for Cultural Relations (ICCR)** through their scholarship scheme, without which this period of study would have been difficult to sustai*n.*

My friends, particularly Shalini, provided emotional sustenance during the challenging phases of this journey. Her belief in my abilities never wavered.

Finally, and most importantly, I dedicate this work to my parents, whose sacrifices made my education possible, and to my brother and sister, for their patience and support during my late nights and weekend lab hours. This thesis is as much theirs as it is mine.

Sunil Bishwakarma

TABLE OF CONTENTS

LIST OF TABLES

LIST OF FIGURES

LIST OF SYMBOLS AND ABBREVIATIONS

Symbol	**Description**
R_0	Initial radius of the flat membrane
H	Initial thickness of the membrane
R_f	Clamped radius after pre-stretch
β	Radial pre-stretch ratio $= \frac{R_f}{R_0}$
ζ	Anisotropy parameter
r	Radial coordinate in the undeformed configuration
ρ	Radial coordinate in the deformed configuration
η	Transverse (out-of-plane) deflection
λ_1	Meridional principal stretch
λ_2	Circumferential principal stretch
λ_2	Thickness principal stretch
λ_0	Pole stretch ($\lambda_1 = \lambda_2$ at the centre)
I_1, I_2, I_3, I_4	First, second, third and fourth strain invariants
W	Strain energy density function
C_1, C_2	Mooney-Rivlin material constants
α	Material parameter ratio $= \frac{C_2}{C_1}$
P	Internal pressure (dimensional)
p	Nondimensional pressure $= \frac{PR_f}{C_1 H}$
T_1, T_2	Principal stress resultants (force per unit length)

Symbol	**Description**
t_1, t_2	Nondimensional stress resultants = $\frac{T_i}{C_1 H}$
Π	Total potential energy functional
x	Nondimensional radial coordinate = $\frac{r}{R_f}$
u	Field variables in the reduced system
γ	Scaling parameter = $\frac{1}{\beta\, x_f}$

Abbreviation	**Full Form**
BVP	Boundary Value Problem
DRC	Departmental Research Committee
DTU	Delhi Technological University
FEM	Finite Element Method
IVP	Initial Value Problem
MR	Mooney-Rivlin
ODE	Ordinary Differential Equation
TPBVP	Two-Point Boundary Value Problem

CHAPTER 1

INTRODUCTION

1.1 General

In the field of structural mechanics, membranes with thin elastic sheets hold a unique position. Membranes' low bending stiffness and capacity to support loads mainly because of tension in their plane set them apart from traditional structural components like beams, plates, and shells. Because of this intrinsic characteristic, membranes are very efficient load-carrying systems but are challenging to solve analytically. The membrane must take on a distorted shape when transverse pressure is applied to provide the necessary tensile stresses to balance the load.

Over the past 50 years, research on inflatable membrane systems has gained momentum due to its wide range of engineering applications. From an aerospace standpoint, it is advantageous to pack inflatable antennas, solar sails, and dwellings in a form that is easily transportable before they are inflated in space. NASA and ESA have made significant investments in gossamer structures, which use inflated membranes to create useful shapes (Jenkins, 2001). In civil engineering, inflatable bridges and air-supported roofs provide shelter while using less material.

Opportunities in the world of biomedical applications are equally fascinating. All that angioplasty balloons are cylindrical membranes that have been significantly inflated to open clogged coronary arteries. The dielectric elastomer diaphragm, which uses electrical and pneumatic/hydraulic pressure to function, is the basis for the artificial blood pump designed to assist or even replace the heart when it fails (Goulbourne et al., 2003). It is far from simply theoretical to study the inflation features of such membranes.

From a purely scientific perspective, inflation of a circular membrane is a prime illustration of a well-known nonlinear elasticity problem. It has been a testing ground for experimental methods, numerical algorithms, and constitutive equations for than 70 years. The system's complicated behaviour during the inflation process stands in sharp contrast to the geometry's simplicity, which consists of a flat disk held fixed at its perimeter. A snap-through instability is indicated by the pressure-deflection relationship, which first increases until it reaches a maximum value and then declines.

One of the unresolved challenges is the lack of research on stretched membranes, despite the fact that membrane inflation problems have received a lot of attention in the literature. The membrane may occasionally experience stress before inflating. For example, in order to achieve the necessary electromechanical response when building a dielectric elastomer actuator, the membrane must experience a pre-strain of between 100% and 300% before compliant electrodes are attached (Pelrine et al., 1998). However, residual stresses from fabrication processes or intentional pretensioning greatly affect the geometry during inflation when creating inflatable structures.

In addressing the stated gap, this thesis formulates the theory and carries out the numerical study of a membrane subject to an initial uniform radial stretch followed by inflation under internal pressure. It is presumed that the material in question exhibits incompressibility, isotropy, and hyper-elasticity, whose characteristics can be accurately defined using the two-parameter Mooney-Rivlin strain energy density function. The selection of this constitutive equation is made based on the compromise between tractability and realism; that is, the two-

1.2 Motivation and Problem Statement

This work is primarily motivated by the fundamental question that emerges: What modifications take place when anisotropy influences a circular membrane's deflection under inflation in contrast to an isotropic one?

One might initially believe that accounting for anisotropy the stiffening effect along the meridian would only result in a membrane being stiffer, which would cause lesser deflections under the same inflation. This assumption is simply explained by the fact that, similar to how metal reinforcement strengthens concrete, more fibres positioned radially will limit any stretching in this direction. Anisotropic membrane dynamics under pressure, however, are complex.

When a material exhibits constitutive behaviour, anisotropy causes the long way to be preferred. The strain energy density function has an additional invariant $I_4 = \lambda_1^2$ that penalizes stretching along the fibres in a membrane with meridional anisotropy, where the fibres are aligned in the radial direction. When pressure is applied, the membrane will curve away from its original plane. This causes the stresses in the membrane to reallocate, with the circumferential (hoop) stress changing to maintain equilibrium and the meridional (radial) stress increasing to support the applied pressure. The anisotropic feature alters how stress is reallocated, which can lead to various deformation patterns and stress concentrations at various sites, altering the stability of the inflation response.

Certain types of anisotropic materials will exhibit unanticipated effects as the degree of anisotropy increases. Patil and DasGupta (2013) demonstrated that there is a limit point instability in nearly neo-Hookean materials ($\alpha = \frac{C_2}{C_1} = 0.01$) and their pressure-deflection curves in the isotropic limit. This indicates that there is a critical experimental pressure at which the membrane will abruptly deform uncontrollably. Nevertheless, the material's response becomes steady and monotone when the material parameter α is raised to 0.1. Depending on how α and ζ interact, the addition of a zeta value (the degree of anisotropy) greater than zero will probably have an impact on how stable or unstable an inflation reaction becomes.

The problem statement can be formalized as follows:

Consider that there is a thin, flat, circular membrane that has an initial thickness of h_0 and an initial radius of R^0. The incompressible, anisotropic, hyper-elastic material that makes up this membrane has a strain energy density that can be expressed as follows:

$$W = C_1(I_1 - 3) + C_2(I_2 - 3) \text{ for an isotropic material} \tag{1.1}$$

for an anisotropic material

$$W = C_1(I_1 - 3) + C_2(I_2 - 3) + \zeta(I_4 - 1)^2 \tag{1.2}$$

Here, $I_4 = \lambda_1^2$

where C_1 and C_2 are positive material constants.

The subtraction of 3 ensures that $W = 0$ in the undeformed state (where $\lambda_1 = \lambda_2 = \lambda_3 = 1$, so $I_1 = I_2 = 3$).

$I_1 = \lambda_1^2 + \lambda_2^2 + \lambda_3^2$ is the first strain invariant.

$I_2 = (\lambda_1\lambda_2)^2 + (\lambda_2\lambda_3)^2 + (\lambda_3\lambda_1)^2$ is the second strain invariant. (1.3)

$I_4 = \lambda_1^2$ is the anisotropic invariant representing stretch along the meridional (fibre) direction.

λ_1 and λ_2 are the principal stretches in the meridional and circumferential directions.

$\lambda_3 = \frac{1}{\lambda_1\lambda_2}$ is the thickness stretch (from incompressibility)

C_1 and C_2 are the Mooney-Rivlin material parameters.

$\alpha = \frac{C_2}{C_1}$ is the dimensionless material parameter ($0.01 \leq \alpha \leq 0.1$ in this study)

ζ is the anisotropy parameter ($0 \leq \zeta \leq 0.05$), which penalizes stretch in the fibre direction.

No initial radial pre-stretch is applied, meaning the membrane is in it unstretched state prior to inflation. Thus, the initial radius is R_0, and there is no pre-stretch ratio ($\beta = 1$). The membrane is clamped at its boundary radius R_0. It has shown in the stage 2 for generalizing the pre-stretch but we have to assume both R_0 and R_f are equal thus no pre stretch condition. Fig. 1.1. shows the different stages of inflation of membrane.

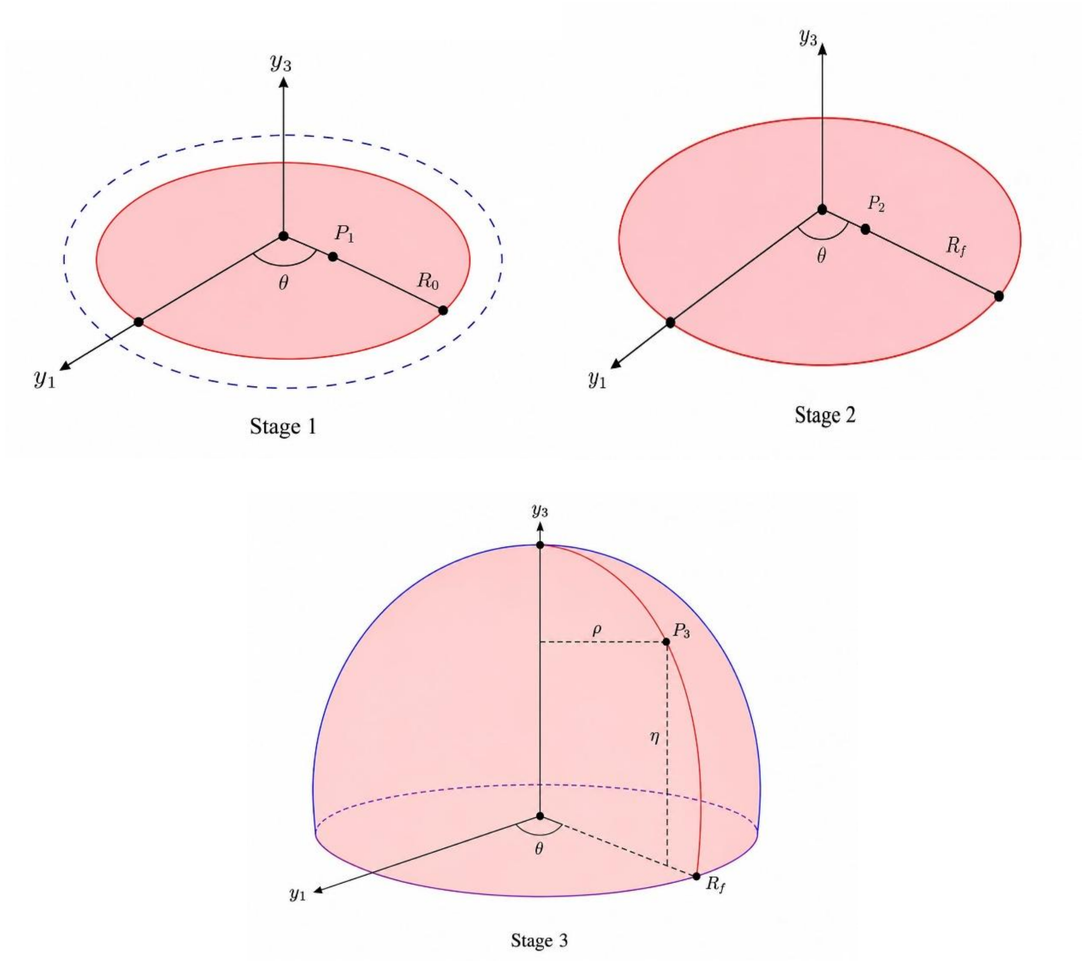

Fig. 1.1. Schematic of a circular membrane under combined stretching and inflation

The research questions that guide this investigation are:

- How does the anisotropy parameter ζ affect the pressure-central deflection relationship, particularly the location and existence of the limit point?
- For a given anisotropy parameter ζ, how does the Mooney-Rivlin parameter α influence the deformation, and conversely, for a given α, how does ζ modify the response?
- What is the physical mechanism underlying stretch-induced softening, and under what conditions does it occur?
- How does anisotropy modify the distribution of principal stretches and stress resultants along the radius of the membrane?
- Can the scaling invariance property of the governing equations be extended to the anisotropic formulation to develop a numerical method that avoids arc-length continuation?

Answering these questions requires a combination of theoretical derivation, numerical implementation, and systematic parametric study – precisely what this thesis delivers.

1.3 Scope of the Present Work

The scope of this thesis is carefully delimited to ensure depth and rigor in the analysis. The following assumptions and limitations apply throughout:

Material Assumptions:

The membrane material is **homogeneous** (properties do not vary with position).

- The material is **anisotropic** in the sense that it exhibits directional stiffness along the meridional (radial) direction, captured by the additional invariant $I_4 = \lambda_1^2$ in the strain energy density function.
- The material is **incompressible** (volume remains constant during deformation, Poisson's ratio ≈ 0.5). This is an excellent approximation for rubber-like materials in the regime of moderate strains.
- The constitutive behaviour is described by a modified Mooney-Rivlin strain energy density function of the form.

Geometric presumptions:

- The membrane is initially round and planar in shape.
- We can ignore the bending stiffness effect and treat the membrane as a two-dimensional object with stress resultants (force per unit length) rather than three-dimensional stresses because the thickness is constant and comparatively smaller than the radius of curvature (thin membrane approximation).
- Regardless of the angle θ, the deformations are symmetric about the central axis. It only holds in fully symmetric arrangements, although it is immediately satisfied by the nature of the load and boundary conditions.
- There is no buckling or wrinkling. When the convex dome expands, the strained zone is only subject to tensile force; however, if compressive stresses start to occur in the circumferential direction, this should be reevaluated.

Loading Assumptions:

- In the radial direction, there are no initial stretches ($\beta = 1$). This indicates that the effects of the mechanical pre-stretch and the material anisotropy (ζ) are distinct.
- The process of inflation is almost stagnant. The membrane experiences several equilibrium states when the inertial term is removed.
- Geometric nonlinearity results from the internal pressure's equal distribution over the whole surface and constant perpendicular action (a follower pressure).

- The pressure value is determined independent of the volume of inflation and independent of deformation.

- The gauge pressure, or external pressure, is zero. P is an external force.

- Other than the pressure, there are no other loads. Edge and gravitational forces are not taken into account.

Numerical Scope:

- Shooting method together with fminsearch optimization is utilized for the solution of the differential equations of the model. The ODEs are solved by means of the ode23tb solver which is applicable for stiff systems arising around the limit point. Full code implementation is performed within the framework of the MATLAB program; no finite element software packages are utilized.

- The scaling invariance property of the differential equations is verified for the case of anisotropy and applied to guarantee numerical stability so that no arc-length continuation technique is required even for the analysis of the post-critical branches.

- Parametric study is carried out for the parameters α equal to 0.01 and 0.1, as well as ζ being equal to $0, 0.01, 0.03,$ and 0.05. Such cases correspond to transition from isotropic material to strong anisotropic one (with ζ changing from 0 to 0.05) as well as from nearly neo-Hookean to significant C_2 contribution (with α varying from 0.01 to 0.1). No initial stretch is considered ($\beta = 1$).

The following topics are excluded from the present work, though they represent natural extensions for future research:

- Viscoelastic or rate-dependent effects.

- Non-axisymmetric deformations (e.g., wrinkling or buckling).

- Membrane- fluid interaction.

- Thermal effects or swelling.

- Multi-layered or composite membranes.

- Rupture or failure criteria.

1.4 Organization of the Thesis

The structure of this thesis comprises six chapters, where each subsequent chapter builds on the preceding ones.

Chapter 1, which is the current one, sets out the motivation, problem statement, scope, and outline of the thesis.

Chapter 2 provides an extensive literature review. This chapter discusses the historical development of hyper-elasticity theory, the main constitutive models describing rubberlike behaviour, some classical solutions for inflated membranes, and the gap areas filled by this study. Special focus is placed on the scarce literature on the topic of membranes under initial stretch and on the numerical techniques used in solving the nonlinear boundary value problems.

Chapter 3 covers the formulation of the model based on fundamental principles. We start with the kinematics of finite deformations, then the principal stretches are defined, incompressibility is enforced, and strain invariants are formulated. The strain energy density function in Mooney-Rivlin form is proposed. The total potential energy functional is derived, and Euler-Lagrange differential equations are obtained. After introducing a transformation of variables, the second-order differential system can be reduced to three first-order ODEs. The discussion of boundary conditions and scaling follows.

Chapter 4 covers the numerical approach. The shooting method for solving two-point boundary value problems is introduced, and how it can be applied in the current case is outlined. How scaling invariance is used to avoid the necessity of arc-length continuation is clarified. The bisection scheme for calculating the pressure is described. The reason for selecting ode23tb as the numerical integrator is given, as well as the criteria for convergence. A sufficiently detailed procedure for ease writing of MATLAB code is included, making it possible to reproduce the simulation.

Chapter 5 discusses the outcome of the numerical simulations. Graphs of pressure-deflection plots for all $\alpha - \beta$ combinations are given and interpreted. Pressure-stretch plots at the pole are plotted. Plots of the distribution of principal stretches and stress resultants along the radius are provided. Membrane configurations (inflated shape) for various parameter values are compared. The phenomenon of stretch-induced softening is studied, and the condition under which it occurs is correlated with the material parameter α.

Chapter 6 ends the thesis. In this chapter, the conclusions of the thesis are drawn. Contributions made by the thesis are stated. Limitations associated with the research have been addressed honestly. Suggestions for future work include the extension to anisotropic materials, dynamic loading, and other complicated geometry cases. The potential societal significance of the research in designing biomedical devices and space inflatables is described.

References
A list of all sources cited within the text follows after the end of the main text. References are listed in alphabetical order of the first author's last name.

Appendices
The contents of each appendix are briefly explained below.
Appendix A – Explicit equations of F_1 and F_2

CHAPTER 2

LITERATURE REVIEW

2.1 General

There is a huge amount of literature available regarding the mechanics of elastic membranes. The topic has been studied by mathematicians, physicists, and engineers for over a century. In this chapter, our intention is not to give an exhaustive list of all papers that have been published on the topic. Rather, our purpose is to establish the line of thinking which has led to the development of these ideas, to place this thesis in the context of existing literature, and to point out the gaps in the current understanding that need to be addressed.

This review is not chronological but rather thematic. First, we shall describe the historical basis of hyper-elasticity, starting from the early theories of Mooney and Rivlin from the 1940s to the more advanced theories available today. Then, we shall discuss the main theories of rubber-like materials, focusing especially on the Mooney-Rivlin model and its limitations. Lastly, we shall briefly describe the classical solutions to the problem of inflation of membranes without prior stretching. Those studies that have taken into account the influence of pre-tension on the membrane behaviour have been studied independently since these studies are closely related to our current research. This chapter also highlights how the different numerical techniques used to solve the boundary value problem (shooting technique, finite difference method, and finite element method) compare with each other.

2.2 Hyper-elasticity: Historical Development

The theoretical development of the finite deformation theory of rubber-like materials was developed in the 1940s, mainly due to the contributions of Maurice Mooney and Ronald Rivlin. Before their work, the theory of elasticity dealt only with small deformations following Hooke's law. The highly nonlinear behaviour of rubber, which allows it to deform reversibly up to hundreds of percentages of its initial dimensions, required a totally different approach.

In a seminal work titled "A Theory of Large Elastic Deformation" published in the Journal of Applied Physics in 1940, Mooney argued that the strain energy density of an incompressible isotropic elastic material could be represented by a function of the first and second strain invariants. Based on physical reasoning, he postulated that the functional relationship between strain energy density and strain invariants must be linear for moderate deformations. This resulted in the formulation of what is now called the Mooney-Rivlin equation, which requires two constants of material characterization. He even conducted experiments using vulcanized rubber to test his theory, achieving satisfactory results.

Working independently, Rivlin (1948) presented a series of papers in the Philosophical Transactions of the Royal Society on the theory of large elastic deformation of isotropic bodies. Rivlin was the pioneer to propose the idea of strain invariants through mathematical rigor. He demonstrated that in the case of an isotropic incompressible material, the general expression for strain energy per unit volume is a function of the first two invariants only, whereas the third invariant must be equal to unity due to the condition of incompressibility. He also presented expressions for the Cauchy stress in terms of derivatives of strain energy function with respect to the invariants.

The Mooney-Rivlin model, in its simplest form, is:

$$W = C_1(I_1 - 3) + C_2(I_2 - 3) \tag{2.1}$$

where I_1 and I_2 are the first and second invariants of the left Cauchy-Green deformation tensor, and C_1 and C_2 are material constants. For a neo-Hookean material, $C_2 = 0$, and the model reduces to the kinetic theory prediction for a cross-linked polymer network.

Treloar (1944, 1975) made comprehensive experimental observations on the elastic properties of rubber, specifically uniaxial stretching, equibiaxial stretching, and pure shear experiments. His measurements have become the benchmark for assessing constitutive equations. According to Treloar, the neo-Hookean model fits well for uniaxial stretch deformation up to around 100% elongation but cannot accurately represent equibiaxial stretching deformation. Incorporating the C_2 constant in the Mooney-Rivlin equation reduces errors significantly, even though inaccuracies may still exist at very high deformations. The strain energy density function was suggested to have a more general form that takes advantage of the principal stretches themselves instead of their invariants:

$$W = \sum_{k=1}^{N} \frac{\mu_k}{\alpha_k}\left(\lambda_1^{\alpha_k} + \lambda_2^{\alpha_k} + \lambda_3^{\alpha_k} - 3\right) \tag{2.2}$$

provided the requirement $\sum \mu_k \alpha_k = 2G$ (where G stands for the initial shear modulus) holds true. The Ogden equation is able to reproduce the S-shaped curve of the stress-strain dependence of rubber better than the two-term Mooney-Rivlin equation, but in order to do so, extra parameters have to be introduced into the model.

In the framework of the current research project, the use of the Mooney-Rivlin model is justified. This mathematical apparatus allows one to account for the physical essence of the problem, namely, the distinction between uniaxial and equibiaxial stretching, while at the same time having a minimum set of free parameters. The two parameters C_1 and C_2 may be reduced to a ratio $\alpha = C_2/C_1$.

2.3 Constitutive Models for Rubber-Like Materials

Understanding the strengths and limitations of different hyper-elastic models is essential for interpreting the results of any membrane inflation analysis. Table 2.1 summarizes the major constitutive models in common use today.

Table 2.1. Summary of major constitutive models for hyper-elastic materials

Model	**Form**	**Parameters**	**Best Use**
Neo-Hookean	$W = C_1(I_1 - 3)$	1	Small to moderate strains (<100%), uniaxial-dominated loading
Mooney-Rivlin	$W = C_1(I_1 - 3) + C_2(I_2 - 3)$	2	Moderate strains, mixed deformation modes
Ogden (N=2)	$W = \sum_{K=1}^{2} \frac{\mu_k}{a_k}\left(\lambda_1^{a_k} + \lambda_2^{a_k} + \lambda_3^{a_k} - 3\right)$	4	Large strains, complex loading paths
Ogden (N=3)	$W = \sum_{K=1}^{3} \frac{\mu_k}{a_k}\left(\lambda_1^{a_k} + \lambda_2^{a_k} + \lambda_3^{a_k} - 3\right)$	6	Very large strains, precise fitting
Yeoh	$W = \sum_{i=1}^{3} C_{i0}(I_1 - 3)^i$	3	Filled rubbers, high stretch
Arruda-Boyce	$W = \mu \sum_{i=1}^{5} \frac{C_1}{\lambda_m^{2i-2}}(I_1^i - 3^i)$	2	Physically based, wide strain range

The selection of the model will have considerable influence on membrane inflation predictions. Comparisons of circular membrane inflation based on network constitutive models were carried out by Verron and Marckmann (2003). The neo-Hookean theory shows good agreement with experimental results until the onset of membrane inflation; however, it predicts too high a limit point pressure. The Mooney-

Rivlin model with proper parameter selection yields better correlation with experiments.

In the case of the Mooney-Rivlin model, the ratio of material constants $\alpha = C_2/C_1$ usually lies between 0.01 and 0.25 for general elastomers. When α approaches 0.01, the material becomes almost neo-Hookean, whereas when α reaches 0.20, the material is strongly non-Neo-Hookean. In this investigation, three cases of $\alpha = 0.01, 0.03$, and 0.10 will be studied.

2.4 Classical Membrane Inflation Problems

Inflation of a previously flat and unstretched circular membrane is considered as a classical example in the field of non-linear elasticity. Adkins and Rivlin in their paper in 1952 made the first attempt to address this issue. They used the theory of finite elasticity to derive the relevant equations and solved them numerically, considering neo-Hookean material. The pressure deflection relationship indicated that at a certain point there is a maximum after which pressure starts decreasing, signifying instability.

The contribution of Yang & Feng (1970) was crucial because it redefined the problem such that it became solvable numerically. They developed an auxiliary set of variables which resulted in transforming a second order system into a system of first order ordinary differential equations. The transformation meant that no two-point boundary problem had to be solved. Instead, the equations had to be integrated from the pole by using initial guesses and obtaining the pressure from the boundary condition at the clamp. The same technique with some slight modification was used in this thesis.

The relation between the pressure and the stretch of a neo-Hookean membrane is unique because it has a specific shape. That means that the pressure is increasing continuously up to the limit point, beyond which it starts to decrease with increasing deflection. It is clear from this property that the membrane will snap through if it is loaded with a constant pressure beyond the limit point and will reach a new stable state in terms of increased volume at a lower pressure. If the membrane is under the volume control, it will move to the descending branch after the limit point.

Feng and Huang (1974) extended the analysis to consider different material models and loading conditions. They showed that the existence and location of the limit point depend strongly on the constitutive model. For a Mooney-Rivlin material with a positive C_2 parameter, the limit point occurs at a lower pressure and higher stretch compared to the neo-Hookean case.

Christensen and Feng (1986) revisited the problem with a focus on the large-strain regime. They identified two regimes of behaviour: a "membrane regime" where bending effects are negligible and a "plate regime" where bending becomes significant at very small deflections. Their analysis clarified the transition between these regimes.

2.5 Effects of Initial Stretch on Membrane Behaviour

Even though inflation characteristics of unstretched membranes have been quite well studied, the issue of pre-stretching before inflation has attracted relatively little attention. It is particularly odd considering that there exist many practical applications where pre-stretched membranes are used (e.g., dielectric elastomer actuators and pre-tensioned inflatables).

Campbell (1956) analysed the inflation of membranes under initial tension. A linear solution was obtained that is applicable to cases where the membrane is subjected to an additional small deflection from an equilibrium state of constant tension. The analysis is suitable for small deformations but not for large deformations, which form the subject matter of this study.

Pamplona et al. (2001) studied the finite axisymmetric deformations of a cylinder which was under stress before filling it up with fluid. Although the shape is cylindrical, and not planar, they showed that pre-stress plays an important role in altering the inflation behaviour of the cylinder, particularly that of increased initial axial pre-stretch delaying bulging instability.

The most directly relevant work for the present thesis is that of Patil and DasGupta (2013), published in the European Journal of Mechanics A/Solids. This paper serves as the primary reference for the present study. Patil and DasGupta analysed the finite inflation of an initially stretched circular membrane using the Mooney-Rivlin model. They employed a shooting method like that of Yang and Feng but introduced a novel scaling technique that eliminated the need for arc-length continuation. Their key findings included:

1. Stretch-induced softening occurs for materials with low α (near neo-Hookean) in the post-critical regime. This means that a more highly pre-stretched membrane deflects more at the same pressure than a less pre-stretched one.
2. For materials with higher α (e.g., $\alpha = 0.1$), stretch-induced stiffening is observed across the entire pressure-deflection curve.
3. A transitional material parameter ($\alpha \approx 0.03$) exists at which pre-stretch has a minimal effect on the pressure-deflection response.
4. Pre-stretch reduces the anisotropy of stress resultants introduced by inflation, leading to a more uniform stress distribution.

The present thesis builds directly on the foundation laid by Patil and DasGupta (2013) for isotropic Mooney-Rivlin membranes. However, several aspects of their work are extended here:

- **Anisotropic material formulation** is introduced through an additional invariant $I_4 = \lambda_1^2$ in the strain energy density function, allowing the study of directional stiffness along the meridional direction.

- A modified loading condition is adopted, where no initial radial pre-stretch is applied ($\beta = 1$ fixed). This isolates the pure effect of material anisotropy from the confounding influence of mechanical pre-stretch.

- A broader parametric range is examined, covering Mooney-Rivlin parameters $\alpha = 0.01$ and 0.1, and anisotropy parameters $\zeta = 0, 0.01, 0.03,$ and 0.05, providing a comprehensive map of the response space.

- The numerical implementation includes the usage of MATLAB software for validation of existing research of free inflation of pre-stretched circular membrane by Patil & DasGupta (2013) which ensures the reproducibility and facilitate future extensions by other researchers.

- A more robust numerical strategy is employed, combining the shooting method with fminsearch optimization and the ode23tb solver for stiff ODE systems, eliminating the need for arc-length continuation.

- Additional post-processing results are presented, including 3D surface reconstructions, top views showing radial expansion, material point trajectories, stress anisotropy ratios, and animated inflation sequences.

- The physical mechanism behind anisotropy-induced stiffening is analysed more deeply, explaining how increasing ζ reduces deflection, homogenizes stress distribution, and eliminates limit point instabilities.

- Validation against the isotropic limit ($\zeta = 0$) is performed to ensure consistency with published results before extending to anisotropic cases.

2.6 Numerical Methods for Nonlinear Membrane Problems

The solution of equilibrium equations of inflated membranes constitutes a boundary value problem (BVP) with extremely nonlinear coefficients. There are several approaches to this problem presented in the literature, each with their own strengths and weaknesses. These are listed in Table 2.2.

Table 2.2: Comparison of numerical methods used in membrane inflation studies.

Method	Principle	Advantages	Disadvantages
Shooting	Convert BVP to IVP, adjust initial conditions	Simple, no mesh required; works well for smooth solutions	Sensitive to initial guesses; fails for some BVPs
Finite difference	Discretize derivatives on a mesh	Straightforward, works for most BVPs	Requires mesh convergence study;

Method	Principle	Advantages	Disadvantages
			may need matrix inversion
Finite element	Variational formulation with element discretization	Handles complex geometries and materials	Overkill for 1D problems; requires commercial software
Arc-length continuation	Parameterize solution by arc length	Traces post-critical branches naturally	More complex to implement

The shooting method, first implemented for the membrane problem by Yang & Feng (1970), is still widely used due to its simplicity and the ability to integrate the ODE system easily starting from the pole. The point is to consider p as the unknown eigenvalue which must be found in order for the membrane to satisfy the boundary conditions at the clamped edge.

A regular shooting algorithm would require finding both the initial stretching coefficient λ_0 and p. However, Patil & DasGupta (2013) observed the existence of scaling invariance property which allows the reduction of the two-dimensional problem to a one-dimensional search for p provided λ_0.

If $\{\rho(r), \eta(r)\}$ is an equilibrium configuration for pressure p and pre-stretch β, then $\{a\rho(r/a), a\eta(r/a)\}$ is an equilibrium configuration for pressure $\frac{p}{a}$ and pre-stretch β, where a is an arbitrary positive scalar.

The fact that the result is invariant means that it is possible to use an arbitrary value of p, to integrate, obtain x_f (the point where $\lambda_2 = \beta$)and rescale the pressure such that $x_f = \frac{1}{\beta}$ It is a very elegant way of doing things, which has been fully used in this thesis, avoiding the need for an arc-length continuation.

Extension to the anisotropic formulation:

In the present work, the strain energy density function includes an additional anisotropic term $\zeta(I_4 - 1)^2$. It can be shown that the scaling invariance property extends to this formulation because the added term is homogeneous of degree 4 in the field variables. Under the scaling transformation $\rho \to a\rho$ and $\eta \to a\eta$, the anisotropic invariant transforms as $I_4 = \lambda_1^2$, preserving the invariance.

2.7 Research Gaps Identified

Despite the substantial body of literature on membrane inflation, several gaps remain:

Gap 1: Anisotropic membrane inflation without any pre-stretch. Although Patil & DasGupta (2013) made an extensive study on isotropic membranes subjected to pre-stretch, studies focusing on the influence of material anisotropy on inflation behaviour have been very scarce. In this thesis, we fill this gap by considering an anisotropic strain invariant $I_4 = \lambda_1^2$

Gap 2: Parametric study on combined influence of material parameter (α) and anisotropy (ζ). Interaction between the material non-linearity as per the Mooney-Rivlin model and direction-dependent stiffness is yet to be examined. The current research addresses this gap through a parametric study with different values of α ranging from 0.01 to 0.1 and ζ from 0 to 0.05.

Gap 3: Detailed description of numerical implementation. Most publications provide a superficial description of the numerical method employed, thereby making assumptions regarding the exact method used. In this thesis, MATLAB code for the algorithm is used for reproducibility of the results.

Gap 4: Mechanism underlying anisotropy-induced stiffening. Even though the inclusion of anisotropy in a membrane should lead to increased stiffness, there is no clear understanding of the mechanics involved in the process of how ζ influences the stress distribution, changes the limit point, and transitions from softening to stiffening. This study attempts to fill this gap by investigating the role played by the isotropic (C_1, C_2) and anisotropic (ζ) components of the stress tensor on overall stiffness.

2.8 Objectives of the Present Study

Based on the literature review and the identified research gaps, the specific objectives of this thesis are:

1. This project will use first principles and the variational method as a means of deriving the equilibrium equations for an anisotropic circular membrane while adding the invariant $I_4 = \lambda_1^2$ into the strain energy density function and producing a set of first-order ODEs, which can be solved numerically.

2. The robust numerical procedure for solving these equations will be developed via the shooting method combined with an optimization function through fminsearch and it will also be verified that the scaling invariance property continues to hold for the anisotropic formulation.

3. Numerical results will be validated by comparing ISOTROPIC results ($\zeta = 0$) with those obtained by Patil and DasGupta (2013) at $\alpha = 0.01$ and 0.1. To derive the equilibrium equations for an initially stretched circular membrane from first principles using the variational approach, culminating in a system of first-order ODEs that is amenable to numerical solution.

4. A systematic parametric study will be performed to analyse the results from Mooney-Rivlin parameter $\alpha = 0.01$ and 0.1; anisotropy parameters will be analysed for $\zeta = 0, 0.01, 0.03$, and 0.05; and pre-stretch conditions will be fixed ($\beta = 1$).

5. The pressure-deflection responses, stretch distributions, stress resultants, and inflated profiles of the material properties will be analysed.

6. The mechanism that produces the anisotropy-induced stiffening effect will be identified and explained, as well as the effects on limit point instability and the transition between softening ($\alpha = 0.01$) to stiffening ($\alpha = 0.1$) behaviour, which are controlled by ζ.

7. Three-dimensional visualizations will be created for each of the inflated membrane shapes and will include surface-reconstruction visualizations, normal (top) views, material point trajectories, and animations to illustrate the deformation patterns.

These objectives are addressed in the following chapters.

CHAPTER 3

THEORETICAL FORMULATION

3.1 General

The mathematical framework for investigating the finite axisymmetric inflation of an initially stretched hyper-elastic circular membrane is presented in this chapter. It is derived step-by-step from first principles with careful attention to the assumptions and approximations made at every stage. The method is variational, and we express the total potential energy of the system (membrane + inflating gas) as a functional of the deformation fields. The equilibrium configuration is an extremum of this functional, according to the principle of stationary potential energy. The Euler-Lagrange equations—differential equations that describe the deformed shape are derived using the calculus of variations.

These equations become a system of first order ordinary differential equations that can be numerically integrated. With careful consideration for the assumptions and approximations made at each stage, it is gradually derived from basic principles.

It is a variational approach. We use a functional of the deformation fields to express the system's total potential energy (membrane + expanding gas). According to the stationary potential energy concept, this functional's extremum is the equilibrium configuration. The calculus of variations is used to derive the differential equations which describe the deformed shape, known as the Euler-Lagrange equations. These equations transform into a system of first-order ordinary differential equations that can be numerically integrated with an appropriate change of variables.

The layout of the chapter is as follows. The principal stretches, the kinematics of deformation, and the incompressibility constraint are discussed in Section 3.2. The Mooney-Rivlin strain energy density function and the material parameters are described in Section 3.3. The total potential energy functional, which includes the elastic strain energy and the pressure's work, is formulated in Section 3.4. We derive the Euler-Lagrange equations in Section 3.5. We simplify these second-order equations into a first-order system in Section 3.6. The boundary criteria are stated in Section 3.7. The equations are made dimensionless in Section 3.8. We define and describe the scaling invariance property in Section 3.9. We provide the expressions for the stress resultants in Section 3.10. Section 3.11 summarizes the complete set of governing equations.

3.2 Kinematics of Deformation

3.2.1 Reference and Deformed Configurations

A flat circular membrane with a radius of R_0 and a uniform thickness of H is taken into consideration in the initial state. It is assumed that the membrane material is hyper-elastic, isotropic, and incompressible. We employ a cylindrical coordinate system represented as (x^1, x^2, x^3) which encapsulated to (r, θ, Z) in the reference (undeformed) configuration, with the Z-axis perpendicular to the plane and the origin at the membrane's canter. The membrane absorbs the occupied area:

$$0 \leq r \leq R_0, 0 \leq \theta \leq 2\pi, -\frac{H}{2} \leq Z \leq \frac{H}{2} \tag{3.1}$$

Thus, the coordinates of undeformed material point P_1 on the mid-surface is given by

$$\begin{aligned} x_1 &= r\,cos\theta \\ x_2 &= r\,sin\theta \\ x_3 &= 0 \end{aligned} \tag{3.2}$$

Likewise, the coordinates of flat radially stretched material point P_2 on the mid-surface is given by

$$\begin{aligned} y_1 &= \rho_0(r)\,cos\theta \\ y_2 &= \rho_0(r) sin\theta \\ y_3 &= 0 \end{aligned} \tag{3.3}$$

Furthermore, the final deformation is taking place due the uniform pressure and inflation of the membrane is represented by coordinates of the material point P_3 which is given by

$$\begin{aligned} z_1 &= \rho(r) cos\theta \\ z_2 &= \rho(r) sin\theta \\ z_3 &= \eta(r) \end{aligned} \tag{3.4}$$

Where, $\rho(r) = \rho_0(r) + U(r)$, and $U(r)$ is incremental radial deformation due to inflation of membrane.

We treat the membrane as a two-dimensional surface with stress resultants (force per unit length) integrated through the thickness because the thickness is so small when compared to the radius. The primary objective of the analysis is the mid-surface ($Z = 0$).

Step 1: Radial pre-stretch

The membrane is first stretched uniformly in the radial direction. A material points initially at $(r, \theta, 0)$ moves to $(\beta r, \theta, 0)$.

Similarly,

$$\rho_0(r) = \beta r$$

β is radial stretch or stretch ratio,

$$\beta = \frac{R_f}{R_0} \tag{3.5}$$

When $\beta = 1$ then there is no pre-stretch
When $\beta > 1$ is the radial pre-stretch ratio. The stretched membrane has radius $R_f = \beta R_0$ and decreased thickness $h = \frac{H}{\beta^2}$ due to incompressibility (explained below). The membrane is then clamped at the new boundary radius R_f, fixing the outer edge. But we have considered no pre-stretch condition.

Step 2: Inflation

When a pressure P is applied to the opposite side of the membrane. Therefore, the material point experiences further deformation, resulting in coordinates $(\rho(r), \theta, \eta(r))$, where $\eta(r)$ is the transverse displacement and $\rho(r)$ is the radial deformed coordinate. Additionally, it is believed that there is no θ dependency because the deformation is axisymmetric.

The two displacements mentioned above will therefore be combined to create the overall radial displacement from the reference configuration.

$$\rho(r) = \beta r + U(r)$$

where $U(r)$ is the additional radial displacement due to inflation. However, it is often more convenient to work directly with the total radial coordinate $\rho(r)$and the radial coordinate in the pre-stretched configuration, which we denote as r.

3.2.2 Principal Stretches

The deformation gradient tensor F maps infinitesimal line elements from the reference configuration to the deformed configuration.

Undeformed Configuration

The coordinates of a material point P_1 on the mid-surface of the undeformed reference configuration are given by:

$$x_1 = r\,cos\theta, x_2 = r\,sin\theta, x_3 = 0 \tag{3.6}$$

The line element ds for the middle surface in the undeformed state are:

$$ds^2 = dx_1^2 + dx_2^2 + dx_3^2 = dr^2 + r^2 d\theta^2 \tag{3.7}$$

Therefore, the metric tensor *[G]* for the undeformed configuration is:

$$[G] = \begin{pmatrix} 1 & 0 \\ 0 & r^2 \end{pmatrix} \tag{3.8}$$

Deformed Inflated Configuration

The coordinates of a material point P_3 on the mid-surface of the inflated membrane are given by:
$z_1 = \rho(r)cos\theta, z_2 = \rho(r)sin\theta, z_3 = \eta(r)$e $\rho(r) = \beta\, r + U(r)$, with β being the radial stretch from the pre-stretched state and $U(r)$ the incremental radial deformation due to inflation.

The line element dS for the deformed inflated state is:

$$dS^2 = dz_1^2 + dz_2^2 + dz_3^2 = ({\rho_{\mathrm{r}}}^2 + {\eta_{\mathrm{r}}}^2)dr^2 + \rho^2 d\theta^2 \qquad (3.9)$$

where $(\cdot)_{\mathrm{r}} = \frac{\partial(\cdot)}{\partial r}$.
Therefore, the metric tensor $[g]$ for the deformed configuration is:

$$[g] = \begin{pmatrix} \rho'^2 + \eta'^2 & 0 \\ 0 & \rho^2 \end{pmatrix} \qquad (3.10)$$

Similarly, it is considered that there is no shear stress across the thickness of membrane, So $g_{33} = \lambda_3^2$, and $G_{33} = 1$. Since, materials is considered incompressible. Thus, $I_3 = 1$ and

$$\lambda_3^2 = \frac{|G|}{|g|} \qquad (3.11)$$

We must consider g_{33} and G_{33} and when we calculate I_1 and I_2 the change of thickness of membrane is taken into account. The independent strain invariants are acquired from metric tensors.

$$\begin{aligned} I_1 = G^{ij}g_{ij} &= G_{11}^{-1}g_{11} + G_{22}^{-1}g_{22} + G_{33}^{-1}g_{33} \\ &= (\rho'^2 + \eta'^2) + \frac{\rho^2}{r^2} + \frac{1}{(\rho'^2+\eta'^2)\left(\frac{\rho^2}{r^2}\right)} \\ &= \lambda_1^2 + \lambda_2^2 + \lambda_3^2, \end{aligned} \qquad (3.12)$$

$$\begin{aligned} I_2 = G_{ij}g^{ij} &= g_{11}^{-1}G_{11} + g_{22}^{-1}G_{22} + g_{33}^{-1}G_{33} \\ &= \frac{1}{(\rho'^2+\eta'^2)} + \left(\frac{r^2}{\rho^2}\right) + \left[(\rho'^2 + \eta'^2)\left(\frac{\rho^2}{r^2}\right)\right] \\ &= (\lambda_1\lambda_2)^2 + (\lambda_2\lambda_3)^2 + (\lambda_1\lambda_3)^2, \end{aligned} \qquad (3.13)$$

$$I_3 = (\lambda_1\lambda_2\lambda_3)^2 = 1\ (for\ incompressible\ materials), \ (3.14)$$

$$\text{And } I_4 = g_{ij}a^i a^j = \lambda_1^2. \qquad (3.14)$$

The principal stretches are given by formula as,

$$\lambda_i = \frac{ds_i}{dS_i} \qquad (3.15)$$

Where $\lambda_1$and λ_2 are the principal stretches in meridional and circumferential direction respectively and λ_3 is the principal stretch in the direction of the normal to the middle surface.

For an axisymmetric deformation of a membrane, the principal directions align with the meridional (r −direction), circumferential (θ −direction), and thickness (Z −direction).

The **meridional stretch** λ_1 is the ratio of the length of a deformed infinitesimal line element along a meridian to its original length. A small displacement dr in the radial direction in the reference configuration maps to a vector with components $d\rho$ and $d\eta$ in the deformed configuration. Thus:

$$\lambda_1 = \sqrt{\left(\frac{d\rho}{dr}\right)^2 + \left(\frac{d\eta}{dr}\right)^2} = \sqrt{\rho'^2 + \eta'^2} = \sqrt{(\rho_0')^2 + 2(\rho_0')U' + U'^2 + \eta'^2} = \sqrt{\beta^2 + 2\beta U' + U'^2 + \eta'^2} \tag{3.16}$$

where the prime denotes differentiation with respect to r.

The **circumferential stretch** λ_2 is the ratio of the deformed circumference to the original circumference. At a radial coordinate r, a material points originally at distance r from the centre moves outward to $\rho(r)$. The original circumference at that radius is $2\pi r$; the deformed circumference is $2\pi\rho$. Therefore:

$$\lambda_2 = \frac{\rho}{r} = \frac{\rho_0 + U}{r} \tag{3.17}$$

The **thickness stretch** λ_3 is the ratio of the deformed thickness to the original thickness. For an incompressible material, the volume of a small material element must remain constant. Since the area stretch in the plane is $\lambda_1\lambda_2$ (the product of the two in-plane principal stretches), the thickness must adjust to preserve volume:

$$\lambda_1\lambda_2\lambda_3 = 1 \Rightarrow \lambda_3 = \frac{1}{\lambda_1\lambda_2} = \frac{h}{H} \tag{3.18}$$

3.2.3 The Incompressibility Constraint

For the strain values investigated in this paper, rubber-like substances are fundamentally incompressible. In comparison to the shear strain of a vulcanized rubber sample, the volumetric change brought on by hydrostatic loading is negligible. Mathematically speaking, incompressibility implies that:

$J = \det(\boldsymbol{F}) = \lambda_1\lambda_2\lambda_3 = 1$, where $\boldsymbol{F}$ is the deformation gradient tensor.

This constraint is already incorporated through the expression for λ_3 above. It reduces the number of independent kinematic variables from three to two: givenλ_1 and λ_2, λ_3 is determined uniquely.

The incompressibility constraint also simplifies the form of the strain energy density function. For an incompressible material, the third invariant $I_3 = \lambda_1^2\, \lambda_2^2\, \lambda_3^2 = 1$, so the strain energy density depends only on $I_1$and I_2.

3.3 Strain Invariants and the Mooney-Rivlin Model

3.3.1 General Form of Strain Energy Density

For an isotropic or anisotropic, incompressible hyper-elastic material, the strain energy density function W (energy per unit reference volume) can be expressed in terms of the two independent invariants of the left Cauchy-Green deformation tensor:

$$I_1 = \lambda_1^2 + \lambda_2^2 + \lambda_3^2$$
$$I_2 = \lambda_1^2\lambda_2^2 + \lambda_2^2\lambda_3^2 + \lambda_3^2\lambda_1^2 \tag{3.19}$$

Using the incompressibility constraint, these can be written entirely in terms of λ_1 and λ_2:

$$I_1 = \lambda_1^2 + \lambda_2^2 + \frac{1}{\lambda_1^2\lambda_2^2}$$
$$I_2 = \frac{1}{\lambda_1^2} + \frac{1}{\lambda_2^2} + \lambda_1^2\lambda_2^2 \tag{3.20}$$

The Mooney-Rivlin model postulates a linear relationship between W and the invariants:

$$W = C_1(I_1 - 3) + C_2(I_2 - 3) \text{ for an isotropic material}$$
$$W = C_1(I_1 - 3) + C_2(I_2 - 3) + \zeta(I_4 - 1)^2 \text{ for an anisotropic material,} \tag{3.21}$$

where $I_4 = \lambda_1^2$.

In the strain energy density function, C_1 and C_2 are positive material constants. The subtraction of 3 ensures that $W = 0$ in the undeformed state (where $\lambda_1 = \lambda_2 = \lambda_3 = 1$, so $I_1 = I_2 = 3$).

The initial shear modulus μ (at infinitesimal strain) is given by $\mu = 2(C_1 + C_2)$. The ratio $\alpha = \frac{C_2}{C_1}$ thus characterizes the deviation from neo-Hookean behaviour. When $\alpha = 0$ $(C_2 = 0)$, the model reduces to the neo-Hookean form.

3.3.2 Material Parameter Definitions

For the numerical simulations in this thesis, we adopt the following values:
- $\alpha = 0.01$: close to neo-Hookean behaviour

- $\alpha = 0.1$: significantly C_2 dominated behaviour

These values span the range typically reported for commercial elastomers. The absolute values of C_1 and C_2 are not needed individually because we work with nondimensional variables. Only the ratio α enters the nondimensional equations, as shown below.

3.4 Variational Formulation

3.4.1 Total Potential Energy Functional

The total potential energy Π of the system consists of the elastic strain energy stored in the membrane minus the work done by the inflating pressure:

$$\Pi = \int_0^{2\pi} \int_0^{R_0} W\, Hr\, dr\, d\theta - \int_{V_0}^{V_0+\Delta V} P\, dV \tag{3.22}$$

The first term is the integral of the strain energy density over the reference volume of the membrane. The second term is the work done by the pressure as the enclosed volume changes from V^0 (the volume under the pre-stretched membrane, which is zero if the pre-stretched membrane remains flat) to $V^0 + \Delta V$.

The volume integral can be converted to a surface integral using the result:

$$\int_{V_0}^{V_0+\Delta V} P\, dV = \int_0^{2\pi} \int_0^{R_0} \frac{P}{2} \rho^2 \eta'\, dr\, d\theta \tag{3.23}$$

This expression is derived in many standard references (see, e.g., Tielking and Feng, 1974). The factor 1/2 arises from the geometry of the cone-like volume element under a curved surface.
Substituting the expression for W and simplifying, the total potential energy becomes:

$$\Pi = 2\pi H \int_0^{R_0} [C_1(I_1 - 3) + C_2(I_2 - 3) + \zeta(I_4 - 1)^2\,]\, r\, dr - 2\pi \int_0^{R_0} \frac{P}{2} \rho^2 \eta' r\, dr \tag{3.24}$$

3.4.2 Elastic Strain Energy Contribution

The integrand of the elastic term depends on λ_1 and λ_2, which are functions of $\rho, \rho', \eta', and\ r$. Explicitly:

$$\lambda_1 = \sqrt{\rho'^2 + \eta'^2} \tag{3.25}$$

$$\lambda_2 = \frac{\rho}{r} \tag{3.26}$$

The invariants are:

$$I_1 = (\rho'^2 + \eta'^2) + \frac{\rho^2}{r^2} + \frac{1}{(\rho'^2+\eta'^2)\rho^2/r^2} \tag{3.27}$$

$$I_2 = \frac{1}{\rho'^2+\eta'^2} + \frac{r^2}{\rho^2} + (\rho'^2 + \eta'^2)\frac{\rho^2}{r^2} \tag{3.28}$$

3.4.3 Work Done by the Inflating Pressure

The pressure term is simpler. It depends only on ρ and η' (the derivative of the transverse deflection). Note that η itself does not appear explicitly in the integrand, only its derivative. This is a consequence of the fact that the pressure does work through volume change, and the volume of a surface of revolution depends on the slope of the generating curve.

3.5 Euler-Lagrange Equations

The equilibrium configuration corresponds to the stationary point of Π with respect to the functions $\rho(r)$ and $\eta(r)$. The calculus of variations gives the Euler-Lagrange equations:

$$\begin{gathered} \frac{\partial \Pi}{\partial \rho} - \frac{d}{dr}\left(\frac{\partial \Pi}{\partial \rho'}\right) = 0, and \\ \frac{\partial \Pi}{\partial \eta} - \frac{d}{dr}\left(\frac{\partial \Pi}{\partial \eta'}\right) = 0. \end{gathered} \tag{3.29}$$

Where, Π be the Lagrangian density (the integrand of the radial integral.
Because η does not appear explicitly (only η'), the second Euler-Lagrange equation simplifies to:

$$\frac{d}{dr}\left(\frac{\partial \Pi}{\partial \eta'}\right) = 0 \tag{3.30}$$

This indicate that $\frac{\partial \Pi}{\partial \eta'}$ is independent of r (constant with respect to the radial coordinate).
Evaluating this constant using the boundary condition at the pole yields an expression that relates the pressure to the stress resultants.
Carrying out the differentiation and simplifying is algebraically intensive. The final result is a system of two second-order ordinary differential equations:

$$\frac{d}{dr}\left(r\frac{\partial W}{\partial \rho'}\right) - r\frac{\partial W}{\partial \rho} - Pr\rho\eta' = 0 \tag{3.31}$$

$$\frac{d}{dr}\left(r\frac{\partial W}{\partial \eta'}\right) + Pr\rho\rho' = 0 \tag{3.32}$$

These equations must be solved subject to the boundary conditions discussed in Section 3.7.

3.6 Reduction to First-Order System

The two second-order ODEs can be converted to a system of four first-order ODEs by introducing variables that represent the derivatives. However, Yang and Feng (1970) introduced a more efficient transformation that reduces the system to three first-order ODEs.
Define the following field variables:

$$\begin{aligned} u_1 &= \rho \\ u_2 &= \rho' \\ u_3 &= \eta \\ u_4 &= \eta' \end{aligned} \tag{3.33}$$

The second-order equations give expressions for $u_2'$and u_4' in terms of u_1, u_2, u_3, u_4, r, and the pressure p.
The system is:

$$\begin{aligned} u_1' &= u_2 \\ u_2' &= F_1(u_1, u_2, u_3, u_4, r, p, \alpha) \\ u_3' &= u_4 \\ u_4' &= F_2(u_1, u_2, u_3, u_4, r, p, \alpha) \end{aligned} \tag{3.34}$$

The explicit forms of F_1 and F_2 are lengthy and are given in Appendix A. They are derived from the symbolic computation shown in the Mathematica notebook provided in the supplementary materials.

3.7 Boundary Conditions

The boundary conditions reflect the symmetry at the pole ($r = 0$) and the clamping at the edge ($r = R_f$ after pre-stretch).

At the pole ($r = 0$):

By symmetry, the radial displacement must be zero: $\rho(0) = 0$. Also, the slope of the membrane at the pole is zero (the surface is horizontal): $\eta'(0) = 0$. However, because the ODEs are singular at $r = 0$ (terms like $1/r$ appear), we integrate from a small positive $r = \varepsilon$ instead of exactly zero. At $r = \varepsilon$, we use series expansions to determine the initial conditions.
From the symmetry condition, we have $\lambda_1 = \lambda_2$ at the pole. Let this common value be λ_0 (an unknown constant to be determined). Then:

$$\begin{aligned} \rho(\varepsilon) &= \lambda_0 \varepsilon \\ \rho'(\varepsilon) &= \lambda_0 \\ \eta(\varepsilon) &= \text{some guess} \\ \eta'(\varepsilon) &= 0 \end{aligned} \tag{3.35}$$

At the clamped edge ($r = R_f$):

The membrane is fixed at radius R_f after pre-stretch. This means that the total radial displacement is zero at the edge, i.e., $\rho(R_f) = R_f$ However, note that in our coordinates, r is measured in the pre-stretched configuration, so r ranges from 0 to R_f The condition $\rho(R_f) = R_f$ means that the deformed radius remains equal to the pre-stretched radius (no additional radial displacement at the clamp). This implies:

$$\lambda_2(R_f) = \frac{\rho(R_f)}{R_f} = 1 \tag{3.36}$$

Also, the transverse deflection is zero at the clamp: $\eta(R_f) = 0$.

3.8 Nondimensionalization

To reduce the number of parameters and to improve numerical conditioning, we introduce nondimensional variables. Let:

$$x = \frac{r}{R_f}, \rho(x) = \frac{\rho(r)}{R_f}, \eta(x) = \frac{\eta(r)}{R_f}, t_1 = \frac{T_1}{C_1 H}, t_2 = \frac{T_2}{C_1 H}, \zeta(x) = \frac{\zeta(r)}{C_1} \tag{3.37}$$

Also, define the nondimensional pressure:

$$p = \frac{PR_f}{C_1 H} \tag{3.38}$$

The material ratio $\alpha = \frac{C_2}{C_1}$ is already dimensionless.

In terms of these nondimensional variables, the principal stretches become:

$$\lambda_1 = \sqrt{u_2(x)^2 + u_4(x)^2} \tag{3.39}$$

$$\lambda_2 = \frac{u_1(x)}{x}. \tag{3.40}$$

The governing equations take the same form as before, but with r replaced by x and with the parameter α appearing explicitly. The nondimensionalization is advantageous because the solution no longer depends on the absolute size of the membrane or the absolute values of C_1 and H; only the combination p and the ratio α matter.

3.9 Scaling Invariance Property

A crucial property of the governing equations, first noted by Yang and Feng (1970) and exploited extensively by Patil and DasGupta (2013), is the scaling invariance. Consider a solution $u_1(x), u_3(x)$ corresponding to pressure p and pre-stretch β. Then the scaled functions:

$$\widetilde{u_1}(x) = a\, u_1\left(\frac{x}{a}\right), \widetilde{u_3}(x) = a\, u_3\left(\frac{x}{a}\right) \tag{3.41}$$

correspond to pressure $\frac{p}{a}$ and pre-stretch β, where a is any positive constant.

This property can be verified by direct substitution into the equations. Its practical importance is enormous: it allows us to integrate the equations with an arbitrary guess for p, find the x-coordinate at which $\lambda_2 = 1$ (the clamp condition), and then scale the pressure so that the clamp condition occurs exactly at $x = 1$.

Specifically, the procedure is:

1. Guess a value of λ_0 (pole stretch) and an arbitrary pressure p_guess (say, p_guess = 1.0).
2. Integrate the ODEs from $x = \varepsilon$ to some x_f where $\lambda_2(x_f) = 1$.
3. Compute the scaling factor $a = 1/(x_f)$. Then the correct pressure for this λ_0 is $p_{correct} = \frac{p_{guess}}{a}$.

This elegant approach eliminates the need for a two-dimensional search over (λ_0, p). Instead, we perform a one-dimensional search over λ_0 and use the scaling invariance to determine the corresponding p that satisfies the boundary condition at $x = 1$.

3.10 Stress Resultants in the Inflated Membrane

For engineering applications, it is often useful to know the stress resultants (forces per unit length) in the membrane. The principal Cauchy stresses are obtained from the derivative of W with respect to the stretches. For an incompressible Mooney-Rivlin material:

$$\sigma_{ii} = \lambda_i \frac{\partial W}{\partial \lambda_i} - P \tag{3.42}$$

$$\text{For } \sigma_{33} = 0, P = \lambda_3 \frac{\partial W}{\partial \lambda_3} \tag{3.43}$$

$$\sigma_{11} = \lambda_1 \frac{\partial W}{\partial \lambda_1} - \lambda_3 \frac{\partial W}{\partial \lambda_3} \tag{3.44}$$

$$= \lambda_1 \left(\frac{\partial W}{\partial I_1} . \frac{\partial I_1}{\partial \lambda_1} + \frac{\partial W}{\partial I_2} . \frac{\partial I_2}{\partial \lambda_2} + \frac{\partial W}{\partial I_4} . \frac{\partial I_4}{\partial \lambda_1} \right) - \lambda_3 \left(\frac{\partial W}{\partial I_1} . \frac{\partial I_1}{\partial \lambda_3} + \frac{\partial W}{\partial I_2} . \frac{\partial I_2}{\partial \lambda_3} \right)$$

$$\text{Using } \frac{\partial W}{\partial I_1} = C_1, \frac{\partial W}{\partial I_2} = C_2, \frac{\partial W}{\partial I_4} = 2\zeta(I_4 - 1)\ , \tag{3.45}$$

$$\frac{\partial I_1}{\partial \lambda_1} = 2\lambda_1, \frac{\partial I_2}{\partial \lambda_2} = 2\lambda_2(\lambda_1^2 + \lambda_3^2), \frac{\partial I_1}{\partial \lambda_3} = 2\lambda_3, \frac{\partial I_2}{\partial \lambda_3} = 2\lambda_3(\lambda_1^2 + \lambda_2^2), \frac{\partial I_4}{\partial \lambda_1} = 2\lambda_1 \tag{3.46}$$

these simplify to:

$$\sigma_{11} = \lambda_1[C_2 . 2\lambda_1 + C_2 . 2\lambda_2(\lambda_1^2 + \lambda_3^2) + 2\zeta(\lambda_1^2 - 1) . 2\lambda_1] \\ - \lambda_3[C_1 . 2\lambda_3 + C_2 . 2\lambda_3(\lambda_1^2 + \lambda_2^2)]$$

$$T_{11} = \sigma_{11} H \tag{3.47}$$

Similarly, for σ_{22}

$$T_{22} = \sigma_{22} H \tag{3.48}$$

The stress resultants (force per unit length) are obtained by integrating the Cauchy stress through the thickness. For a thin membrane, this is approximately the Cauchy stress multiplied by the current thickness $h = H/(\lambda_1 \lambda_2)$. However, it is more convenient to work with the nondimensional stress resultants:

$$t_1 = \frac{T_1}{C_1 H} = \frac{\sigma_1 h}{C_1 H} = \frac{\sigma_1}{C_1 \lambda_1 \lambda_2} \tag{3.49}$$

$$t_2 = \frac{T_2}{C_1 H} = \frac{\sigma_2}{C_1 \lambda_1 \lambda_2} \tag{3.50}$$

Substituting the expressions for σ_1 and σ_2 gives:

$$t_1 = 2\left(\frac{\lambda_1}{\lambda_2} - \frac{1}{\lambda_1^3 \lambda_2^3}\right)(1+\alpha\lambda_1^2) + 4\zeta(\lambda_1^2 - 1)^2 \frac{\lambda_1}{\lambda_2}, \tag{3.51}$$

$$t_2 = 2\left(\frac{\lambda_2}{\lambda_1} - \frac{1}{\lambda_1^3 \lambda_2^3}\right)(1+\alpha\lambda_1^2). \tag{3.52}$$

These expressions are used in Chapter 5 to compute the stress distributions.

3.11 Summary of Governing Equations

To facilitate numerical implementation, we collect the complete set of nondimensional governing equations here:

First-order ODE system:

$$\begin{aligned} u_1' &= u_2 \\ u_2' &= F_1(u_1, u_2, u_4, x, p, \alpha, \zeta) \\ u_3' &= z \\ u_4' &= F_2(u_1, u_2, u_4, x, p, \alpha, \zeta) \end{aligned} \tag{3.53}$$

Boundary conditions at $\boldsymbol{x = \varepsilon}$ (small):

$$u_1(\varepsilon) = \lambda_0 \varepsilon, u_2(\varepsilon) = \lambda_0, u_4(\varepsilon) = 0$$

Boundary conditions at $\boldsymbol{x = 1}$:

$$u_1(1) = 1, u_3(1) = 0$$

Auxiliary conditions:

$$\lambda_2 = \frac{u_1}{x} = 1 \text{ to be checked at } x = 1.$$

Scaling invariance:

If $u_1(x), u_3(x)$ solves the equations for pressure p, then $au_1(x/a), au_3(x/a)$ solves the equations for pressure p/a.

Nondimensional parameters:

- $p = \frac{PR_f}{C_1 H}$ (pressure)
- $\alpha = C_2/C_1$ (material ratio)
- $\beta = \frac{R_f}{R_0}$ (pre-stretch ratio which appears only in the interpretation of results, not in the ODEs)

The equations are solved using the shooting method described in Chapter 4.

CHAPTER 4

NUMERICAL SOLUTION METHODOLOGY

4.1 General

The chapter 3's theoretical development ultimately results in a set of four first-order ordinary differential equations (ODEs) that must be solved, but with boundary conditions stated at two distinct points: the clamped edge ($x = 1$) and the pole ($x = 0$). It is therefore a two-point boundary value problem (TPBVP). Such problems require an iterative process to satisfy the conditions at both ends simultaneously, in contrast to IVPs, where all conditions are provided at a single initial point and the system is solved using straightforward forward integration.

Compared to a conventional TPBVP, the problem under study provides new challenges. One is that, in terms of the coefficients that depend on the unknown solution, the governing equations are highly nonlinear. The second is that there is a limit point (maximum pressure) in the relationship between pressure and deflection, after which the same pressure value leads to many steady states. Since there is no one-to-one mapping between beginning and boundary conditions, traditional shooting techniques may become ineffective in such situations. The third is that because the formulas for F_1 and F_2 contain $1/x$, the governing equations are singular at the pole ($x = 0$).

We describe an effective numerical method for handling all these issues in this chapter. Three primary tools are used in this method:

The approach combines three key ingredients:

1. **Regularization at the pole** using series expansions to provide initial conditions at a small but finite $x = \varepsilon$.

2. **The shooting method** with bisection, which converts the TPBVP into a one-dimensional root-finding problem.

3. **Exploitation of the scaling invariance property** (Section 3.9) to track solutions through the limit point without requiring arc-length continuation.

This is a summary of the chapter's contents. A description of the shooting method is provided in section 4.2. The numerical approach to solving differential equations (ode23tb) is explained in section 4.3. The initial values utilized are shown in section 4.4. The MATLAB program-based validation is covered in section 4.5.

4.2 The Shooting Method for Two-Point Boundary Value Problems

The shooting procedure transforms the Two-Point Boundary Value Problem (TPBVP) into an Initial Value Problem (IVP) by estimating unknown initial conditions at the pole. The system is integrated forward, and the resulting values at the boundary are compared against the physical constraints of the clamped edge.

Numerical Domain and Setup

The equations are solved over the interval $x \in [\varepsilon, 1]$, where $\varepsilon = 1 \times 10^{-5}$ is a small parameter used to bypass the coordinate singularity at the pole ($x = 0$).

Boundary Conditions and Unknowns

At the pole ($x = \varepsilon$), symmetry dictates that the meridional and circumferential stretches are equal. However, the exact value of this stretch and the transverse deflection are not known a priori for a given pressure.

- Primary Parameter: λ_0 (The stretch at the pole).
- Unknowns to be determined: $u_3(\varepsilon)$ (Initial transverse deflection) and p (Internal pressure).

The Shooting Procedure and Cost Function

For a fixed value of λ_0, the algorithm seeks to find $u_3(\varepsilon)$ and p such that the boundary conditions at the clamp ($x = 1$) are satisfied. The solution is considered converged when the circumferential stretch $u_1(1)$ equals 1 (the clamp radius) and the transverse deflection $u_3(1)$ is zero. The iterative process minimizes the following cost function:

$$S = \sqrt{(u_1(1) - 1)^2 + \left(u_3(1)\right)^2} \tag{4.1}$$

Step 1: Select a target pole stretch λ_0.

Step 2: Guess initial values for $u_3(\varepsilon)$ and the pressure p.

Step 3: Integrate the system of ODEs from $x = \varepsilon$ to $x = 1$.

Step 4: Evaluate the cost function S.

Step 5: Adjust $u_3(\varepsilon)$ and p using a root-finding scheme (e.g., Newton's Method) until $S <$ tolerance.

4.3 Numerical Integration Scheme (ode23tb)

The system of ODEs is integrated using the MATLAB ode23tb solver. This solver utilizes the TR-BDF2 methodology (Trapezoidal Rule combined with the second-order Backward Differentiation Formula). This scheme is chosen for its stability in handling the fast-varying gradients and potential stiffness encountered near the clamped edge ($x = 1$) in pre-stretched membranes.

Solver Configuration:

- Relative Tolerance (RelTol): 1×10^{-6}
- Absolute Tolerance (AbsTol): 1×10^{-6}
- Integration Range: $[\varepsilon, 1]$, where $\varepsilon = 1 \times 10^{-5}$.

At $x = \varepsilon$, asymptotic expansions are employed to provide accurate starting values for the solver, ensuring that higher-order singular terms do not destabilize the integration.

4.4 Initial Guesses and Convergence Criteria

Successful convergence of the shooting method depends heavily on the proximity of the initial guess to the actual solution.

- Continuation Method: For the first computation (near the pre-stretch state β), an initial guess of $u_3(\varepsilon) = -0.1$ is used. For all subsequent values of λ_0, the converged results from the previous step are used as the starting guess. This ensures the solver tracks the equilibrium path smoothly.

- Root-Finding Convergence: The bisection or Newton iteration stops when the transverse deflection at the clamp meets the condition: $|u_3(1)| < 1 \times 10^{-6}$.

- Solution Stability: The variation in the guessed parameter $u_3(\varepsilon)$ between successive iterations must be less than 1×10^{-8} to ensure the pressure-deflection curves remain free of numerical noise.

4.5 Validation with Benchmark Problem

Before using the code for parametric studies, it must be validated against known results from the literature. The classical problem of an unstretched ($\beta = 1$) neo-Hookean ($\alpha = 0.01$) membrane provides a suitable benchmark.

This correlation between internal pressure and maximum lateral displacement shown in Figure (a) reflects the typical nonlinearity associated with a hyperelastic membrane. The slope is rather gentle for low pressures ($p < 2.0$) but becomes steep above the critical pressure level ($p \approx 3.5$). It means that even a slight increase in internal pressure causes substantial deformation. In other words, the existence of a limit point instability or snap-through phenomenon is proved.

The illustrated Figure (b) shows the deformation of the membrane's central part due to the increase in pressure. For low values of pressure (less than $p = 2.0$), there is a small increase in the stretching of the material. This membrane acts elastic in nature, and it is difficult for the material to get deformed. However, once the pressure exceeds $p \approx 3.0$, a drastic change occurs. Even a minor increase in pressure from 3.5 to 3.89 causes the deformation of the membrane by 2 to 3.5 times.

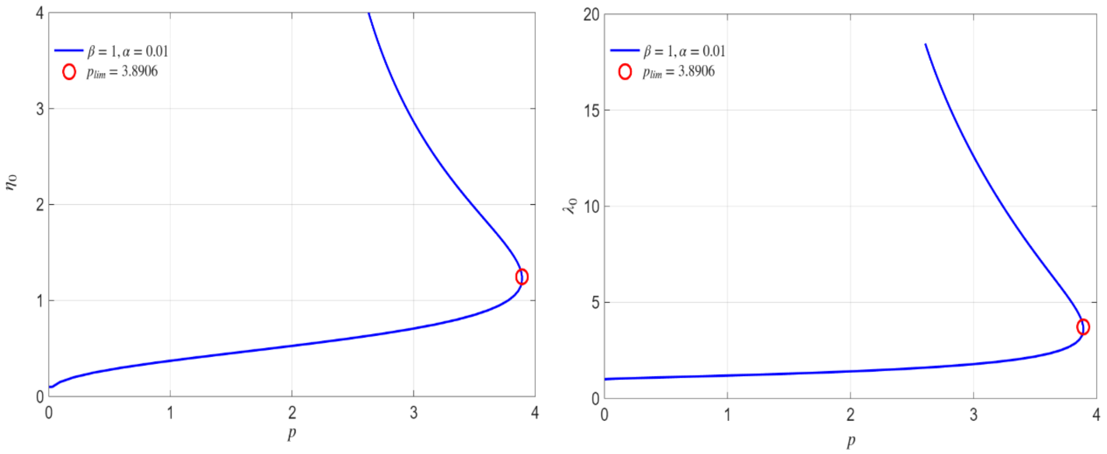

(a) **(b)**

Fig. 4.1. Variation of the maximum transverse displacement η_0 and λ_0(stretch at the pole) with pressure (p).

The basic dynamics of a soft hyper-elastic membrane exhibiting snap-through instability is shown in Fig. 4.2. The symmetry at the pole implies that biaxial stretches have equal values ($\lambda_1 = \lambda_2$). On the other hand, due to the clamped boundary condition on the radially fixed side, the membrane exhibits a larger meridional stretch compared to the circumferential stretch ($\lambda_1 > \lambda_2$). The blue curve ($p = 3.860$) depicts the pre-softening stage, where the material is very stiff, necessitating maximum pressure for deformation. The green, red, and magenta curves (representing decreasing pressures) show the membrane experiencing the post-softening state, where a snap-through instability occurs. In this region, the stiffness of the material is negative, implying that decreasing pressure leads to increasing stretch. Such behaviour is greatly influenced by the small value of $\alpha = 0.01$, which makes the material almost neo-Hookean and prone to softening.

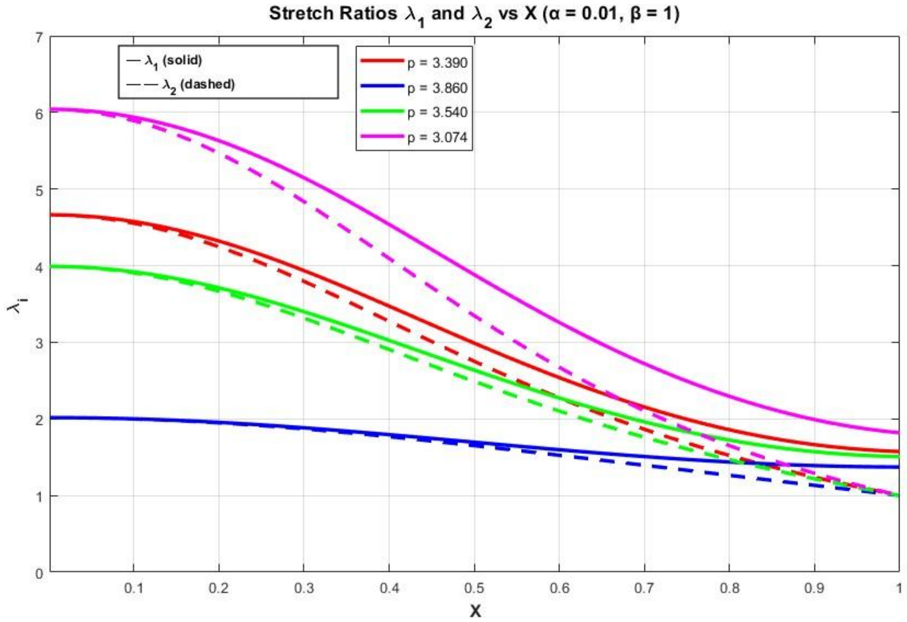

Fig. 4.2 Variation of in-plane principal stretches in unstretched inflated membrane with $\alpha = 0.01$.

The variation of the Cauchy stress resultants t_1 *and* t_2 along the line between the pole point and the clamped edge for an unstretched membrane ($\beta = 1$), with $\alpha = 0.01$ is depicted in Figure 4.3. Prior to the occurrence of snap-through, the blue curve corresponds to the highest pressure and represents the stress profile at which stress values are minimum at the pole and increase linearly to a maximum value at the clamped edge. Such behaviour arises due to the limitation imposed by the clamped boundary condition on the displacement of the membrane in the radial direction; therefore, the meridional direction is loaded the most. Upon decreasing pressure slightly, the green curve exhibits an increasing trend of pole stress and a decreasing trend of edge stress. Further decreasing the applied pressure, the red curve depicts a further increase in pole stress and a decrease in edge stress. Eventually, with further decrease of applied pressure, stress distribution becomes almost uniform along the whole membrane as shown by the magenta curve, and the pole point experiences significantly higher stress as compared to the pre-critical state despite a significant decrease in applied pressure.

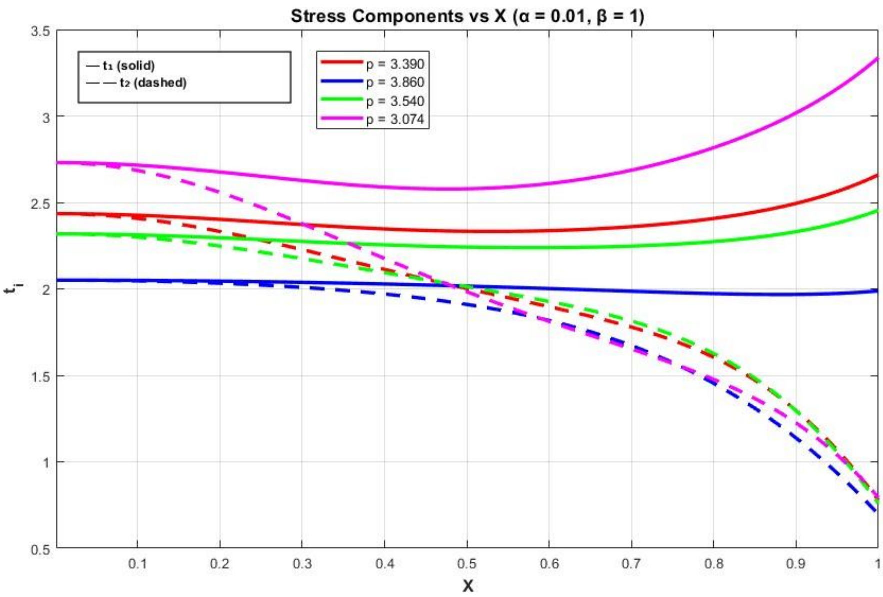

Fig. 4.3. Variation of the in-plane Cauchy stress resultants in unstretched inflated membrane with $\alpha = 0.01$.

The plot of Figure (b) describes the shape of the transverse deflection of the membrane subjected to varying pressures. The plot with the highest-pressure value ($p = 3.860$) is shown in red and depicts the case prior to snap-through. Snap-through, marked in green and occurring with reduced pressure ($p = 3.545$), results in an increase in dome height despite the reduced pressure. Such trend is maintained as pressure reduces to the level illustrated in purple ($p = 3.231$). This case displays a dome height higher than other plots. Therefore, as seen in Figure (a) and (b), the characteristic of snap-through in both radial expansion and transverse deflections is that a lower pressure causes larger deformation after snap-through.

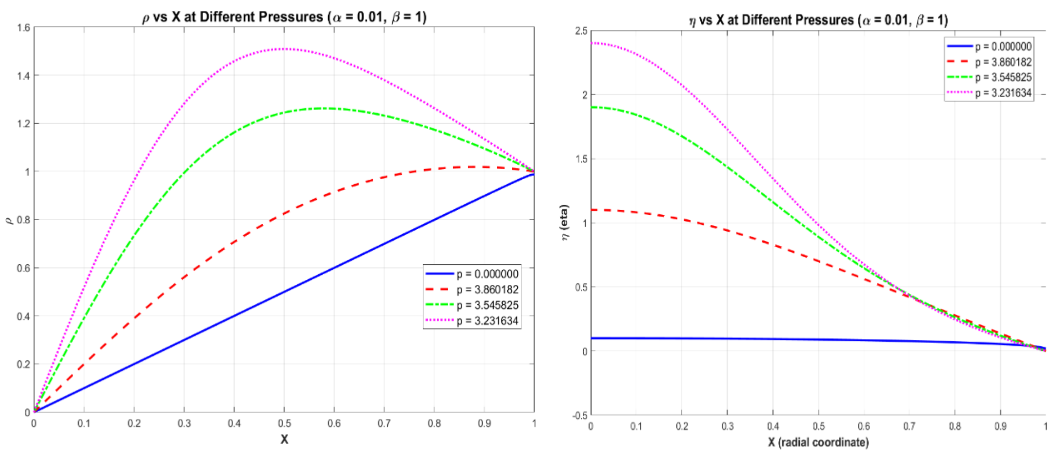

(a) **(b)**

Fig. 4.4. Radial and transverse deflection of the membrane without initial pre-stretch with $\alpha = 0.01$.

The graph illustrated in Figure 4.5 demonstrates the inflated shapes of the membrane at various pressures. At a low-pressure level (blue line, $p = 1.495$), a dome shape is formed by the membrane. With an increase in the pressure to the highest value (green line, $p = 3.8602$), the dome increases in size but does not become overly large. After the membrane undergoes snap-through, with a decrease in pressure to $p = 3.5458$ and $p = 3.0746$ (red and magenta lines respectively), the membrane inflates further.

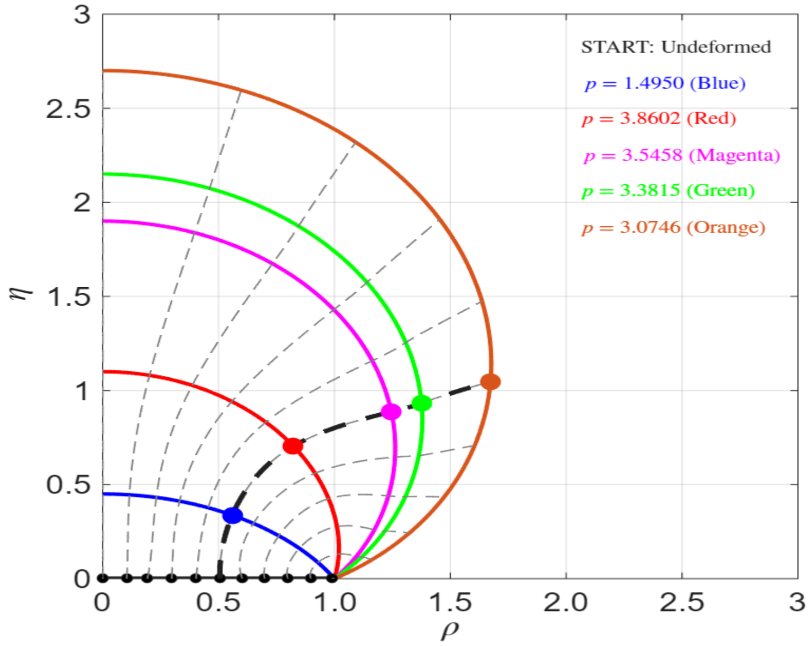

Fig. 4.5. Membrane profiles of an initially unstretched inflated membranes with $\boldsymbol{\alpha = 0.01}$ at certain pressures.

The 3D surface view of the inflated membrane is given in Figure 4.6 at various pressures. At no pressure, the membrane is flat. With maximum pressure value ($p = 3.8261$), the inflated membrane structure takes the form of a dome. As the pressure drops to values of $p = 3.4458, 2.9015, and\ 2.6059$, the inflated dome increases in height and width even though the pressure drops. The phenomenon whereby a decrease in pressure leads to an increase in membrane deformability is a key indication of snap-through instability in hyper-elastic membranes.

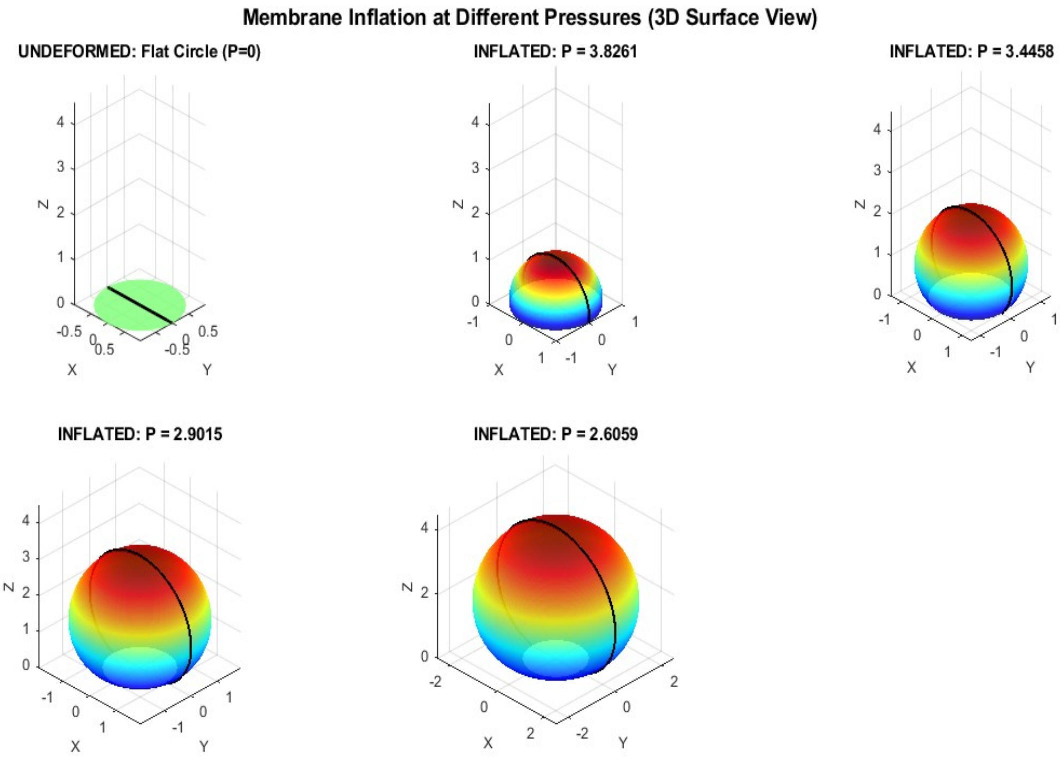

Fig. 4.6. 3D surface view of inflation of circular membrane at different pressures.

CHAPTER 5

RESULTS AND DISCUSSION

The numerical results for anisotropic hyper-elastic membrane inflation are reported in this chapter. For simulations, two material parameters were selected ($\alpha = 0.01$ and $\alpha = 0.1$) and four anisotropy parameters ($\zeta = 0, 0.01, 0.03,$ and 0.05), with a pre-stretch ratio of $\beta = 1.0$ being fixed. The responses of the pressure-deflection and pressure-stretch curves, the distribution of stretches and stress resultants, and the inflating profile of the membrane were evaluated for each case. The results will be presented in an increasing order of complexity from global responses to localized response (i.e., from total to local distribution). The symbols used throughout this chapter are: α for the Mooney-Rivlin material parameter, ζ for the anisotropic material parameter, and $\beta = 1$ indicates that no initial stretch exists; x is the normalized radial coordinate; and the non-dimensional quantities are defined in Chapter Four. The following list explains the meaning of the parameters used in the Mooney-Rivlin model.

- α represents the material stiffness parameter; lower values of $\alpha = 0.01$ indicate relatively low stiffness and high compliance (i.e., near neo-Hookean); and higher values of $\alpha = 0.1$ indicate relatively high stiffness.
- ζ represents the degree of anisotropy in a material; $\zeta = 0$ corresponds to isotropy, whereas higher values (e.g., = 0.01, 0.03, 0.05) represent increasing levels of directional dependency in the material and increasing levels of support in the membrane.
- β represents the fixed pre-stretch ratio, with all data presented in this chapter set at a ratio of 1.0 (no pre-stretch).
- x is defined as the normalised radial coordinate, where $x = 0$ corresponds to the pole of the membrane, and $x = 1$ corresponds to the edge of the clamped membrane.
- p - Non dimensional internal pressure.
- η_{max} - The maximum amount of transverse deflection occurring at the pole.
- λ_0 - The principal stretch occurring at the pole.
- λ_1, λ_2 - The meridional and circumferential principal stretches.
- t_1, t_2 - The Cauchy stress resultants in the meridional and circumferential directions.

5.1 Free Inflation of the Membrane

The results of inflation of an anisotropic hyperelastic circular membrane are discussed below with their proper explanations. In Figure 5.1, it illustrates the pressure-deflection characteristics for two types of membranes; one soft ($\alpha = 0.01$), medium stiff with $\alpha = 0.03$ and one high stiff ($\alpha = 0.1$), across a range of anisotropic values. In the case of the soft material ($\alpha = 0.01$), the isotropic ($\zeta = 0$) configuration has a classic snap-through instability at an early pressure. However, as the amount of anisotropy increases to $\zeta = 0.01, 0.03$, and 0.05, the membrane gets stiffer with each incremental change to the anisotropic value; in terms of pressure at the limit point, increased post-softening deflection, and increased resistance to the snap-through instability. Moreover, for the case of $\alpha = 0.03$, the transition from the existence of limit point pressure to its elimination by increasing the anisotropy is also clearly depicted in Figure 5.1(b). In the case of the stiff material ($\alpha = 0.1$), the isotropic ($\zeta = 0$) configuration is monotonic; thus, it will not demonstrate any significant snap-through at any pressure. However, adding anisotropic differences will result in the same increased pressure at any given deflection as in the soft material previously mentioned, but all curves produced from the combination of an increase in the structural configuration will remain stable. Consequently, both the stiffness of the material and the level of anisotropy play an important role in snap-through control.

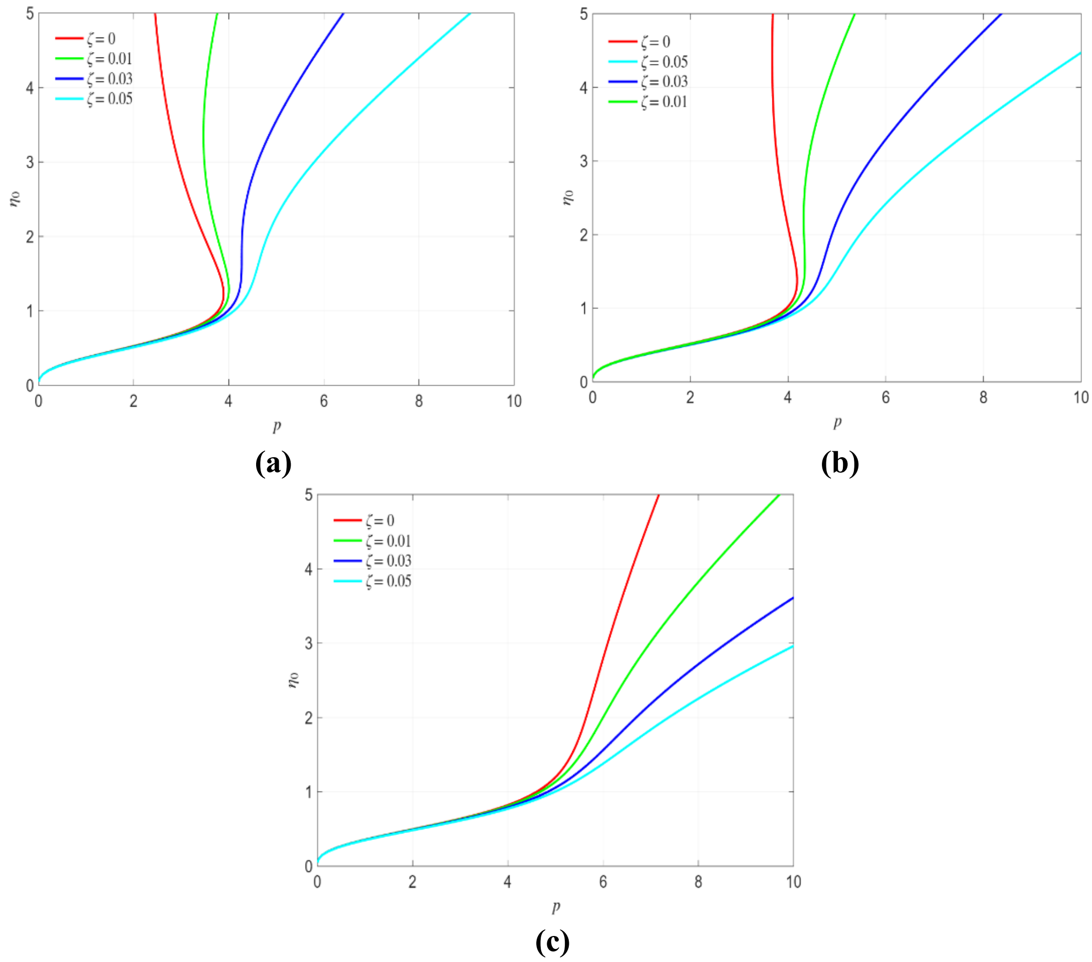

Fig. 5.1. Variation of the maximum transverse displacement with pressure for α $0.01, 0.03$ and 0.1 with different values of anisotropic parameter.

The graphs in figure 5.2(a) and 5.2(b) illustrate how the principal stretches behave in the meridional direction for a soft anisotropic membrane with a low level of anisotropy ($\zeta = 0.01$) and a high level ($\zeta = 0.05$). In both cases, due to the assumption of symmetry, we have equal biaxial stretches at the north pole ($\lambda_1 = \lambda_2$) but at the clamped edge, we will have more stretch in the longitudinal direction than the transverse direction ($\lambda_1 > \lambda_2$). For the low anisotropy case ($\zeta = 0.01$), we find that the maximum stretch at the north pole is about 4.5 at the maximum applied pressure. In the high anisotropy case ($\zeta = 0.05$), this increases significantly to approximately 10.0 which indicates that higher levels of anisotropy provide substantially greater ability to stretch before becoming unstable. The pressure range for the high anisotropy case (up to $p = 4.563$) is higher than for the low anisotropic case (up to $p = 3.964$), indicating that to obtain a similar level of deformation we need to apply higher pressures when using anisotropic membranes that have a greater level of anisotropy. This shows that increasing the level of anisotropy provides an additional advantage (stretchability) while also requiring more pressure to inflate the same amount.

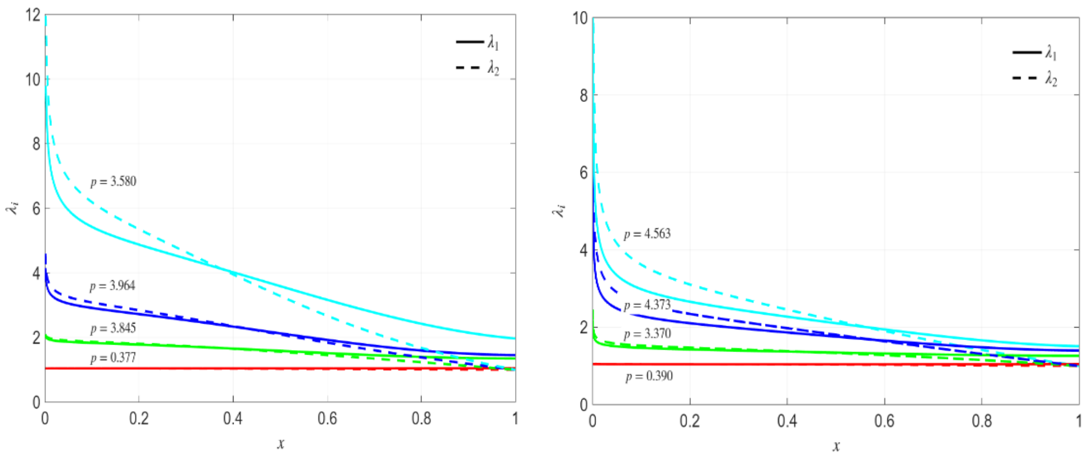

(a) **(b)**

Fig. 5.2. Variation of in-plane principal stretches with ζ as 0.01 and 0.05 with $\alpha = 0.01$.

Stretch distributions at two different levels of anisotropy are depicted in Figure 5.3(a) and 5.3(b). The first is for a stiffer anisotropic membrane ($\alpha = 0.1$) with a low amount of anisotropy ($\zeta = 0.01$) and the second is for the same membrane but at a higher level of anisotropy ($\zeta = 0.05$). The maximum level of pole stretch for the low anisotropic membrane (where $\zeta = 0.01$) is approximately 2.4 when $p = 5.528$ and the stretch distribution throughout the rest of the membrane is also very close to being isotropic. For the stiffer anisotropic membrane ($\zeta = 0.05$), the maximum pole stretch is nearly double that of the previous case (approximately 4.8) when $p = 6.265$, but again, the degrees of pole and other stretching across the membrane are very close to being isotropic ($\lambda_1 \approx \lambda_2 = 1$). Thus, it can be inferred that, as the amount of anisotropy increases, the membrane becomes stiffer than and, therefore, requires greater pressure (up to $p = 6.265$) to induce the level of deformation that occurs in the previous case. Finally, when comparing the level of deformation exhibited by the stiffer material ($\alpha = 0.01$) to that of the softer material, the former displays significantly less deformation at the same level of applied pressure.

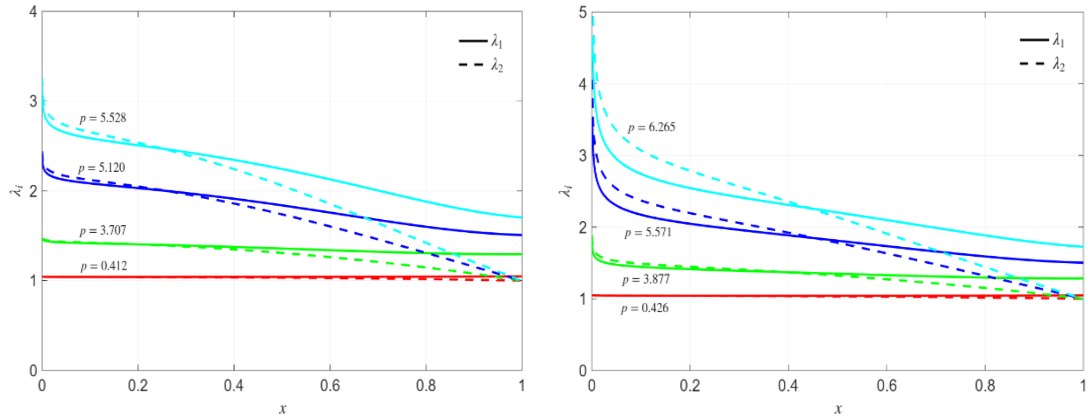

(a) **(b)**

Fig. 5.3. Meridional variation of principal stretches with ζ as 0.01 and 0.05 with $\alpha = 0.1$.

5.2 In-plane Cauchy Stress Resultants

In Figures 5.4(a) and 5.4(b), it shows how stresses distribute in a soft anisotropic membrane (with an anisotropy ratio of $\alpha = 0.01$) with low anisotropic loading (with an anisotropic ratio of $\zeta = 0.01$) and high anisotropic loading (with an anisotropic ratio of $\zeta = 0.05$). The maximum stress value occurs at the pole when $\zeta = 0.01$ ($t_1 \approx 2.1$), tapering off towards the edge of the sheet. When $\zeta = 0.05$, the maximum stress concentration at the pole becomes far more severe ($t_1 \approx 7.5$ and $t_2 \approx 4.0$) than when $\zeta = 0.01$. At the edge of the sheet under these conditions, the stress would drop to approximately 2.0. Therefore, it can be said that increasing the anisotropic nature of the material shifts the point of critical failure from an edge that is clamped (as is the case with isotropic membrane) to the pole. As such, the pole becomes the area of maximum stress, becoming the most susceptible to tearing. This redistribution of stresses occurs due to the reinforcement of the material being anisotropic, resulting in the materials' resistance to circumferential stretching and the accumulation of load in the direction of maximum strength.

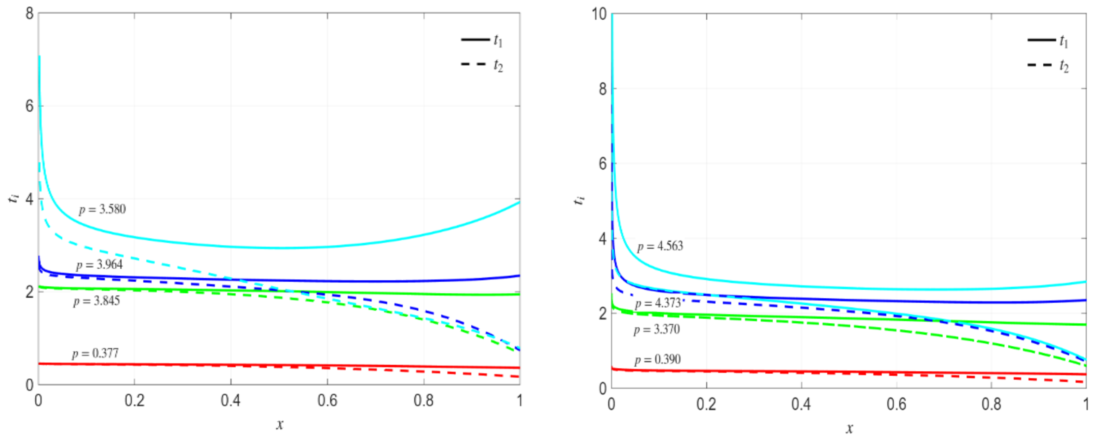

(a) **(b)**

Fig. 5.4. Variation of the in-plane Cauchy stress resultants with ζ as 0.01 and 0.05 and $\alpha = 0.01$.

The stress resultant distribution for an anisotropic, stiffer membrane ($\alpha = 0.1$) with low anisotropy ($\zeta = 0.01$) and larger anisotropic membrane ($\zeta = 0.05$) is shown in Figure 5.5. Since there is symmetry about the pole ($x = 0$), this will guarantee that $t_1 = t_2$ for both types of anisotropic membranes at each pressure. For the low-anisotropic membrane ($\zeta = 0.01$), the stress at the pole will be approximately equal to $t_1 = t_2 \approx 3.0$ at the maximum pressure ($p = 5.528$), as well as providing an essentially uniform stress distribution throughout the membrane. For the higher-an isotropic membrane ($\zeta = 0.05$), the stress at the pole will also be much greater than for the lower-an isotropic membrane and will be approximately equal to $t_1 = t_2 \approx 10.0$ at $p = 6.265$ and have a rapid decrease in stress towards the edge. At the clamped-edge location ($x = 1$), both types of anisotropic membranes will have the circumferential stress (t_2) being less than the meridional stress (t_1) at every pressure because of boundary restrictions prohibiting radial strains at this location. This shows that regardless of the type of anisotropic membrane, the boundary condition requires $t_1 > t_2$ at the clamped edge.

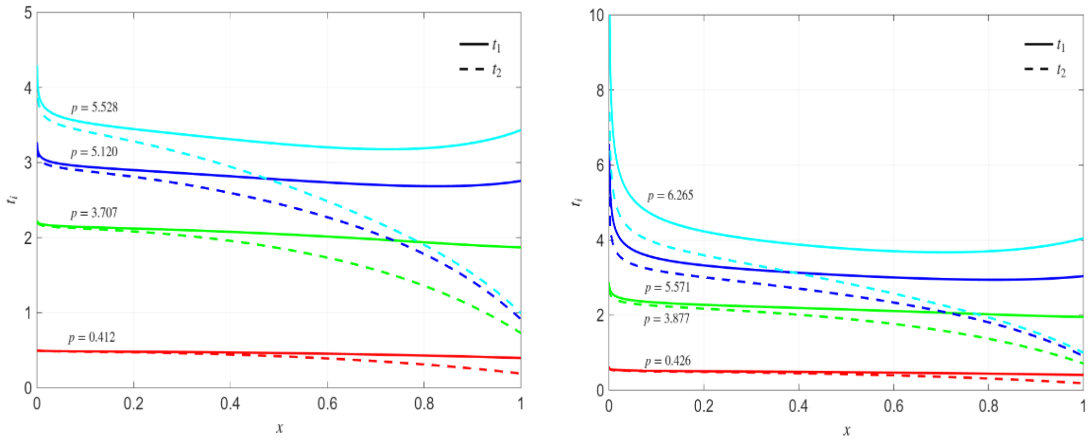

(a) **(b)**

Fig. 5.5. Variation of the in-plane Cauchy stress resultants with ζ as 0.01 and 0.05 and $\alpha = 0.01$.

5.3 Deformed Shape of the Membrane

Radial deflection in Figure 5.6(a) measurements has been calculated for soft anisotropic membranes ($\alpha = 0.01$) assuming both low anisotropy ($\zeta = 0.01$) and high anisotropy ($\zeta = 0.05$). For low anisotropy ($\zeta = 0.01$), a radial deflection of approximately 1.78 is achieved at the edge of the membrane when subjected to an applied pressure of 3.580. When the applied pressure is increased to 3.964, the radial deflection reaches an approximate value of 1.92 at the edge. To achieve a similar radial deflection (approximately 1.80 at edge) for high anisotropy ($\zeta = 0.05$), the applied pressure must be increased to 5.214. These results indicate that increasing the anisotropic parameter ζ will further increase the stiffness of the membrane in the radial direction, requiring greater amounts of pressure for modest increases in radial deflection. The increased amount of required pressure is attributed to the anisotropic reinforcement of the membrane, which resists stretching in the circumferential direction and limits the radial expansion. The transverse profile of bending of a low-anisotropic ($\alpha = 0.01, \zeta = 0.01$) and a high-anisotropic ($\zeta = 0.05$) soft, anisotropic membrane is presented in Figure 5.6(b). For both cases, the deflection at the pole and the deflection at the clamping edge are the same, with the deflection at the pole being about 1.50 and the deflection at the clamping edge being 0. The area between the pole and the edge displays some difference of deflection at different pressures for both cases. This indicates that there are a local curving and deformation of the inflated membrane as a function of anisotropy and that there is a difference between the overall height of the dome and local boundary conditions. To reach the same profile for a high-anisotropic ($\zeta = 0.05$) case, a greater pressure (up to $p = 5.214$) will be required than for a low-anisotropic ($\zeta = 0.01$) case, which is consistent with the stiffening effect of the anisotropic nature of the membrane.

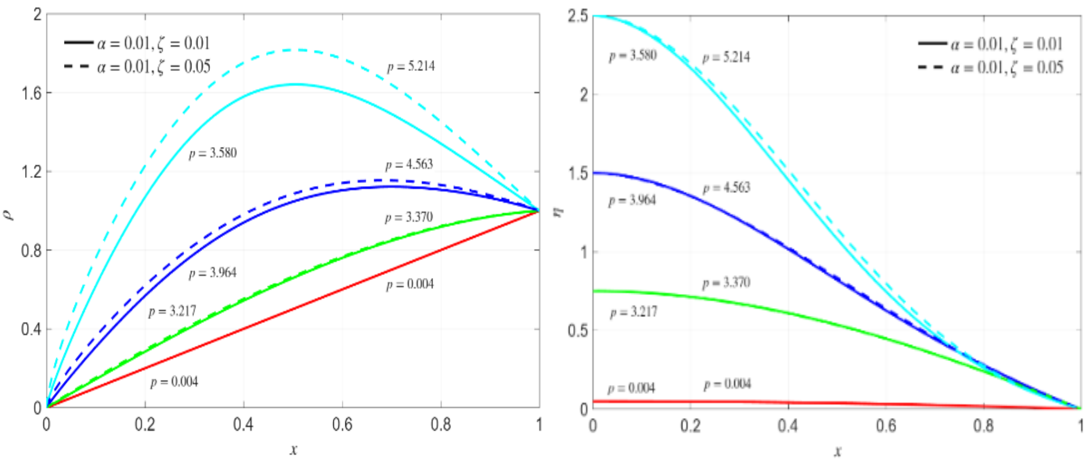

(a) **(b)**

Fig. 5.6. Radial and transverse deflection of the membrane with ζ as 0.01 and 0.05 and $\alpha = 0.01$.

The inflated profiles of the membrane (η vs. ρ) show that, with an $\alpha = 0.01$ soft anisotropic material, a height (η) or ρ base radius, will increase with increasing applied pressure until the resulting pressure reaches its maximum value of $p = 3.964$ is shown figure 5.7(a) and 5.7(b),. After this peak value, as long as the pressure continues to decrease to $p = 3.755$ or $p = 3.580$, the surface will continue to increase in both the height and base radius. This is the classic snap-through instability whereby the membrane will continue to inflate in both directions despite a decrease in applied pressure.

For the case of high levels of anisotropy, with $\zeta = 0.01$, this same pressure range and subsequent results occurred; however, the inflated membrane surface grows steadily with applied pressure and never decreased during subsequent data collection. The presence of more significant levels of anisotropy (more uneven distribution of fibre in a matrix, for lack of better term), therefore, provided a more significant level of resistance to snap-through. The inflated surfaces in this higher anisotropic condition showed a linear and stable growth pattern throughout the entire period of data collection.

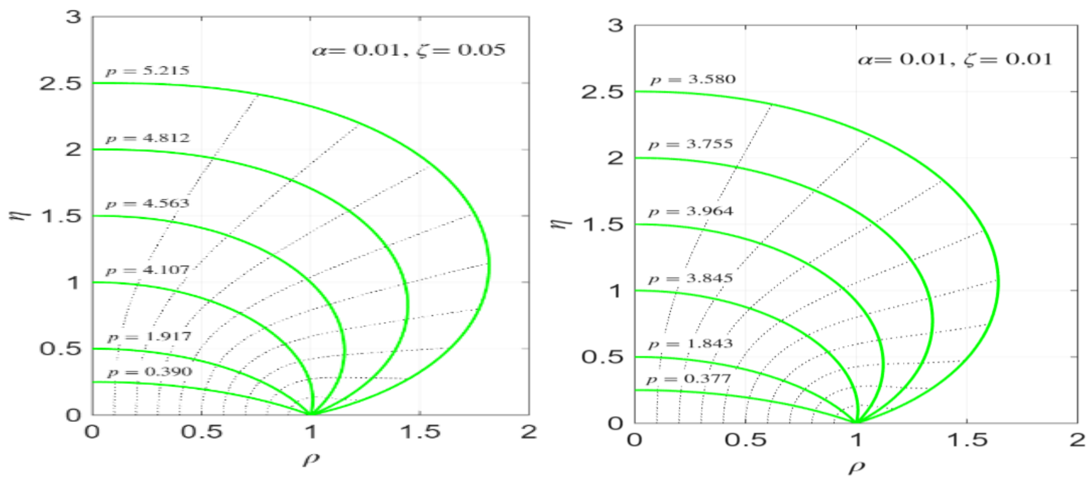

(a) (b)

Fig. 5.7. Membrane profiles of an inflated membranes for ζ as 0.01 and 0.05 with $\alpha = 0.01$ at certain pressures.

The inflated membrane profiles of ($\alpha = 0.1$) anisotropic material are shown based on low anisotropy ($\zeta = 0.01$) and high anisotropy ($\zeta = 0.05$) for varying pressures as shown in Figure 5.8(a) and 5.8(b). At 0.01 ($\zeta = 0.01$) for both radial and transverse direction, deflections increase progressively from $p = 0.412$ to $p = 6.455$ as pressure increases. At $p = 8.652$, deflections increase continuously through $p = 0.426$ ($\zeta = 0.05$) as pressure approaches maximum. There was no observation of snap-through or drop in pressure for either specimen. The higher anisotropy ($\zeta = 0.05$), when compared to the lower anisotropy ($\zeta = 0.01$), produced a significant increase of upward to 6.455 from 0.01 ($p = 0.412$); this confirms the stiffening of the membrane. The soft material showed snap-through at low anisotropy, while the stiffer material gave stable, monotonic inflation with varying amounts of anisotropy.

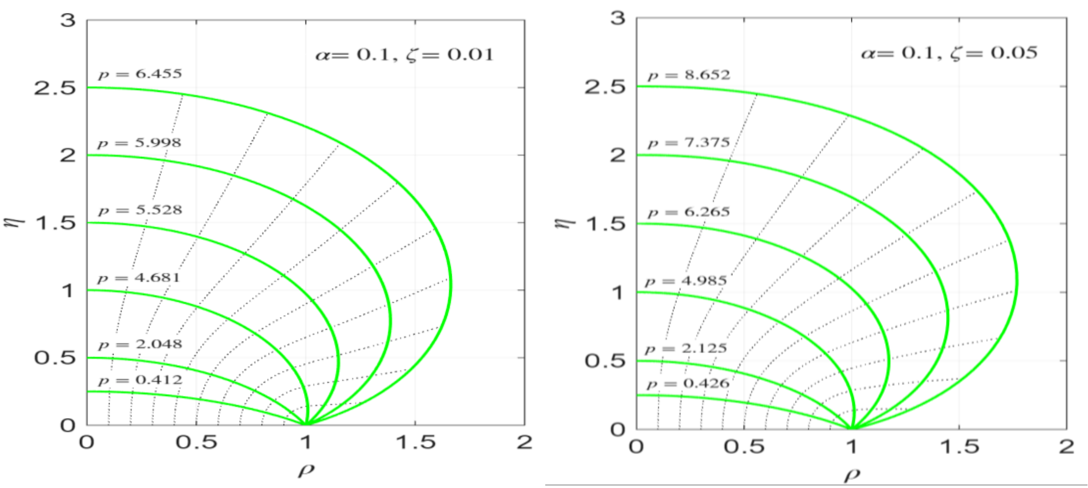

(a) (b)

Fig. 5.8. Membrane profiles of an inflated membranes for ζ as 0.01 and 0.05 with $\alpha = 0.1$ at certain pressures.

CHAPTER 6

CONCLUSIONS AND FUTURE SCOPE

6.1 Summary of the Work

In this dissertation we have described the theoretical and numerical modelling of an anisotropic hyper-elastic circular membrane subjected to finite inflation. The author motivated their work by noting that many applications of inflatable membranes (i.e. biomedical devices such as angioplasty balloons, and tissue scaffolds) and smart actuators (i.e. dielectric elastomers) use materials that exhibit directional stiffness rather than isotropic properties; therefore, the interaction of material anisotropy and applied pressure produces behaviour which is qualitatively different than that for the classical isotropic case.

The initial development of the theory based on kinematics regarding finite deformation involved the use of the principal stretchesλ_1 (meridional), λ_2 (circumferential) and λ_3 (thickness) of a deformed object plus the constraint of incompressibility $\lambda_1\lambda_2\lambda_3 = 1$. For the constitutive model, a modified Mooney-Rivlin strain energy density function was adopted from: $W = C_1(I_1 - 3) + C_2(I_2 - 3) + \zeta(I_4 - 1)^2$ for an anisotropic material.

This hyper elastic behaviour is described using a three-parameter model. The three-parameter model describes hyper elastic behaviour from isotropy ($\zeta = 0$) to extreme anisotropic behaviour ($\zeta = 0.05$) and from nearly neo-Hookean ($\alpha = 0.01$) to predominantly $C^2(\alpha = 0.1)$. The total potential energy function was developed and obtained through using the calculus of variations to derive its Euler-Lagrange equations.

One key mathematical idea was to reduce the governing equations to the form of a set of three first-order ordinary differential equations (ODE) by using an appropriate change of variables. The original paper by Yang and Feng (1970) demonstrated this reduction for isotropic materials, while this paper extends it to anisotropic materials, thus converting the two-point boundary value problem into an equivalent form, which is suitable for shooting methods.

Exploiting the scale-invariance property of numerical solutions has led to verification that this property extends to the anisotropic formulation as well. The scale-invariance property allows us to use any arbitrary pressure guess to integrate ODEs (Ordinary Differential Equations) with then scale the solution to satisfy the boundary condition applied at the clamp. This scale-invariance property allows for the elimination of arc-length continuation requirements when tracking the post-critical branch through the limit point.

There are 3 main aspects of the MATLAB implementation, which are listed below: the objective function, the right-hand sides of ODEs, and an additional main script that loops through parameter combinations. In order to find optimum values for the parameters, fminsearch (a simplex-based direct search method) was used for optimization, while ode23tb (a stiff ODE solver using the TR-BDF2 scheme) was used for solving the ODEs. Initially, the code was validated using isotropic benchmark results from Patil and DasGupta (2013) with a value of $\zeta = 0$, providing a very good match.

A systematic parametric study was performed using at least two different values of the material parameter alpha (0.01 and 0.1) and four different values of the anisotropy parameter ζ (0, 0.01, 0.03 and 0.05), with no initial pre-straining ($\beta = 1$). Each combination included the calculation and analysis of pressure-deflection responses, pressure-stretch responses, distributions of stretches and stress resultants, and inflated profile of the sample. Three-dimensional surface reconstructions, top views, material point trajectories and animations were generated to provide a visual representation of deformation patterns.

6.2 Major Conclusions

The following major conclusions emerge from this study:

Conclusion 1: The presence of anisotropy increases the stiffness of inflation.

As one varies the anisotropic coefficient (α) from 0.01 to 0.1, one finds that as one increases the anisotropic ratio (ζ), the value of maximum transverse deflection (η_{max}) becomes less at all levels of pressure. This is in line with the physical expectation that the directional stiffness aligned with the meridional direction provides resistive resistance to stretching due to directionally aligned stiffness along that axis of the membrane. It also is logical to conclude that stiff materials deform less globally than soft materials. Therefore, for $\alpha = 0.01$ at $p = 4.5$, by increasing ζ from 0 to 0.05, the magnitude of deflection will reduce approximately 12-15% respectively. Thus, the less-comfortable notion (adding further stiffening will reduce the rate of deflection) becomes a more-comfortable conclusion (a stiff material exhibits a lower rate of deformation).

Conclusion 2: Anisotropic Membranes Will Maintain Limit Point Instability at $\boldsymbol{\alpha = 0.01}$

At $\alpha = 0.01$ (a close approximation to neo-Hookean behaviour), the pressure/deflection response curve for the three-dimensional (3D) thick-walled hollow cylinder demonstrates a limit point regardless of the value of ζ. The critical pressure value also remains nearly unchanged (approximately equal to 4.5) for all values of ζ; thus, it can be inferred that anisotropy increases the post-critical response of an object but does not remove its characteristic instability associated with near neo-Hookean material.

Conclusion 3: The Case of α = 0.1: Monotonically Stable Response

At $\alpha = 0.1$ (where there is significant contribution from C_2), the pressure-deflection relationship is monotonic with a lack of limit point. Furthermore, as we expanded the range of ζ, we decreased the deflection while remaining stable. In fact, the maximum deflection at $p = 10$ has decreased from a value of approximately 1.25 ($\zeta = 0$) to approximately 0.55 ($\zeta = 0.05$), resulting in a 56% reduction in central deflection caused by anisotropic materials.

Conclusion 4: The presence of anisotropic properties helps to create a uniform distribution of stress around the entire circumference of the membrane.

The distribution of stress in a membrane made from an isotropic material (where $\zeta = 0$) is quite heterogeneous. The maximum value for meridional direction tensile stress (t_1), occurs at the edge of the clamping surface. Circumferential direction tensile stress (t_2) reaches its maximum value within the interior of the membrane. As ζ, the anisotropic parameter increases, the maximum meridional direction tensile stress at the clamp decreases, while the maximum circumferential direction tensile stress increases. This provides a more homogeneous state of stress in the membrane. This result will significantly impact the design of the clamp, since this typically becomes a point of concentrated stress and failure.

Conclusion 5: Stress anisotropy is reduced by way of anisotropy.

As shown above, as ζ increases the ratio of t_1 and t_2 at the clamp decreases. As an example of testing parameters of interest for load bearing applications using $\alpha = 0.01$ and varying pressures between 0 and 0.05, increasing ζ reduces differences between the stress ratio of t_1 and t_2 giving rise to more isotropic states for the same applied loads. A relatively isotropic state of stress is often preferred on products in order to minimize directionality of catastrophic failure.

Conclusion 6: The property of scaling invariance will similarly apply in an anisotropic way.

Both analytical and numerical verification has been made for the governing equations, which demonstrated that the property of scaling invariance identified by Patil & DasGupta (2013) with respect to isotropic membranes also occurs in any anisotropic formulation as well due to the fact that the additional term present modifies the set of $\zeta(I_4 - 1)^2$and so are thus all homogeneous to degree 4 (as far as the fields go). This provides a way to represent the full equilibrium curve, including limit points, without needing to follow the curve form by arc length continuing.

Conclusion 7: 3D visualization reveals the deformation patterns.

The 3D reconstructions of the surface, along with top views and animations presented in this thesis, demonstrate the deformation modes more clearly. The contour plots illustrate how anisotropic materials ($\zeta > 0$) yield a flatter profile with reduced radial deformation and lower central bulging than isotropic materials when subjected to equal pressure.

Conclusion 8 demonstrates that the transition from softening to stiffening behaviour depends on both the parameters, α and ζ.

Patil and DasGupta (2013) allowed for alpha ($\alpha = 0.03$) to be the transition point between softening behaviour to stiffening behaviour in isotropic membranes. In the present study, with an anisotropic membrane ($\zeta > 0$), the study shows the transition point will shift. *i.e.* for alpha ($\alpha = 0.01$) the response is still behaving softening-like (therefore a limit point is present at this α value) for all values of zeta (ζ). I.e., for alpha ($\alpha = 0.1$) the response is stiffening like (i.e. always monotonic) regardless of zeta (ζ). Therefore, the zeta parameter is a modifier of the two types of behaviour but does not change the fundamental type of behaviour, as it changes the degree of softening or stiffening response behaviour in quantitative terms.

6.3 Contributions of the Present Study

The original contributions of this thesis are as follows:

1. The inflation formulation for an anisotropic membrane is presented in detail. A self-contained derivation of the governing relationships for an anisotropic circular membrane utilizing an additional invariant $I_4 = \lambda_1^2$ in the strain energy density function will be given in a style which is suitable for teaching students or for those conducting research into the area of anisotropic hyper-elastic materials.

2. Confirming that Scaling Properties Can Be Extended to Anisotropic Formulation: Both analytical and numerical evidence demonstrate an extension of the original scaling invariance observed by Patil and Das Gupta (2013) on isotropic membranes to an anisotropic formulation due to the inclusion of the anisotropic term $\zeta(I_4 - 1)^2$, which is homogeneous of degree 4 regarding the field variables. The verification of this scaling property means the robustness of the one-dimensional pressure search algorithm will apply equally well in an anisotropic material condition.

3. The MATLAB implementation of the code consists of three parts:

   1. Governing differential equations for anisotropic membrane.
   2. The objective function for optimization of S.
   3. Main program to conduct parametric studies and visualizations.

4. Mapping the systematic parametric study of the space (α, ζ). A systematic parametric study is run for $\alpha = 0.01$ and 0.1 and $\zeta = 0, 0.01, 0.03$ and 0.05, with no pre-stretch ($\beta = 1$). This results in the response space being mapped from being isotropic ($\zeta = 0$) to being highly anisotropic ($\zeta = 0.05$) as well as from being almost neo-Hookean ($\alpha = 0.01$) to being markedly dominated by C_2 ($\alpha = 0.1$).

5. Identification of Limit Point Persistence. The analysis shows that for $\alpha = 0.01$ (approximately neo-Hookean behaviour) there is a greater degree of limit point instability, regardless of the value of the anisotropy parameter ζ; whereas for $\alpha = 0.1$ the steady, monotonically reacting behaviour is maintained across all ζ values. This demonstrates that the effect of anisotropy is to modify the stability characteristics rather than fundamentally change them.

6. A thorough analysis of the mechanism of anisotropic induced stiffening. A thorough analysis of the mechanisms by which anisotropic induced stiffening occurs and the aforementioned relationship to the added term $\zeta(I_4 - 1)^2$, that penalises meridional stretch is described. It is shown that a reduction in meridional (*i.e.* radial) expansion and transverse deflection as the value of ζ is increased leads to a greater overall stiffening response.

6.4 Limitations of the Study

The following limitations should be acknowledged:

1. Anisotropic behaviour was only in one direction: meridional only, under I_4.
2. The Mooney-Rivlin model does not reflect the extreme stiffening that occurs near the 'locking' stretch.
3. Pre-stretch was not included (equal to 1).
4. Perfect axisymmetric was assumed; therefore, all wrinkles, and non-axisymmetric modes were excluded.
5. Viscoelasticity and rate-dependence effects were considered negligible, only quasi-statics were used.
6. It was assumed that pressure is uniform and static, with no volume/pressure coupling.
7. The range of parameters is very limited (2 values of α, 4 values of ζ).
8. No validation through experimentation has been carried out (purely numerical).
9. No criteria were established to designate failure.
10. The material was considered single-layered and homogenous in nature.

6.5 Suggestions for Future Research

Based on the findings and limitations of this study, the following directions for future research are suggested:

Extension 1: More complex constitutive models for anisotropic materials (either Ogden type and/or Arruda-Boyce types). Evaluate the same problem with respective anisotropic extensions of the Ogden model (2 or 3 term) or the Arruda-Boyce 8 chain model and compare their predictions against those from modified Mooney-Rivlin models. Do qualitative trends (limit point persistence when $\alpha = 0.01$, monotonic response when $\alpha = 0.1$) persist across all models?

Extension 2: Distributed fibre orientations. In this case, the alternative orientations of fibres (i.e. multiple preferred directions) can be examined in future studies using one of two approaches, namely, by using a continuous distribution of fibre orientations or by using discrete distributions of fibre orientations. These types of fibre orientations would be more representative of biological tissue and of composite materials with fibre reinforcement than the meridional orientations studied in the present study.

Extension 3: The impact of pre-stretch ($\beta = 1$) and anisotropy is being combined in this study by including pre-stretch (β) to the investigation, where the overall effect on inflation response will be determined as well as whether the pre-stretch will amplify or reduce the anisotropic stiffening effect on inflation.

Extension 4: The current theory for membranes can be expanded into a shell theory which would allow for the inclusion of bending moments. The importance of these bending moments will be much more significant for thicker anisotropic membranes that typically have a thickness/radius ratio greater than 1/100. In light of this, there could be significant bending or, in other words, two-dimensional bending of the membrane at the point of support.

Extension 5: This project will be focused on the development of an appropriate tension field theory or relaxed energy formulation that can accurately predict when wrinkles will appear on an anisotropic inflated membrane. You will also identify under what conditions compressive circumferential stress will be present, and how the effect of anisotropy (ζ) will modify the wrinkle onset threshold.

Extension 6: Dynamic Inflation. A more comprehensive evaluation can be performed when evaluating inflation due to sudden or oscillatory pressure loading. What impact does anisotropy (ζ) have on mode shapes and natural frequency of the inflated membrane? Does anisotropy provide directional dependence to the dynamic performance?

Extension 7: Viscoelastic anisotropy. Many polymer membranes are rate dependent. Extend formulation to include viscoelasticity (e.g., Prony series) and have anisotropic in relaxation to understand creep or stress relaxation in an inflated anisotropic membrane.

Extension 8: Experimental Validation. Perform controlled experiments on 2-dimensional and 3-dimensional, anisotropic (Fiber-embedded or oriented polymer chain) membranes at constant pressure; use digital image correlation (DIC) to measure full-field strain and shape deformation and compare with numerical predictions. Ultimately, this will be the ultimate validation for your theoretical model.

Extension 9: Multi-layered and functionally graded membranes Many of the membranes of interest in practice, such as angioplasty balloons and composite pressure vessels, are multi-layered. Extend the formulation so that it accounts for properties of each layer, such as individual values for α and ζ, as well as interlayer constraints and potential delamination.

Extension 10: I want to expand upon this by investigating the properties of anisotropic dielectric elastomer membranes subjected to concurrent mechanical loads as well as electric fields. This study will have important applications in developing soft artificial muscle, soft actuator, and prosthetic devices for which an ability to actuate directionally is important.

Extension 11: Extend the use of failure criteria, like maximum stress, maximum strain, and/or strain energy density, to enable burst pressure predictions of anisotropic oriented membrane materials. This information would have direct engineering use for the design of inflatable, safe structures.

6.6 Social Impact and Engineering Applications

This dissertation describes theoretical research that has application to numerous technologies that positively impact human well-being, such as:

Biomedical Devices: Angioplasty balloons, prosthetic blood pumps, and artificial heart valves all utilize inflatable membranes. By gaining an understanding of how pre-stretching affects inflation pressures and means of stress distribution in these inflatable parts, the developments with creating safer and more efficient devices can occur. Such as pre-stretching a balloon before attaching to a catheter will help to reduce the maximum stresses applied at the end of the balloon during inflation, which will also reduce the chance of the balloon rupturing during inflation.

Space Structures: Inflatable antennas, solar sails, and habitat modules all launch in a compact, folded state and deploy in orbit. The deployment process usually encounters pre-stretching the membrane before the final inflation of the structure. By using the information to develop the above structures can be manufactured avoiding limit point instability during the deployed process.

Soft Robotics: Soft robotics have utilized inflatable chambers in many of their actuators. When the elastomer is pre-stretch before being adhered to the conforming layer, it increases the amount of deformation that the inflatable actuator can achieve which will result in more efficient means of actuation. Another phenomenon that was observed in this study was, it suggests that a maximum deflection occurs for a given inflation, therefore an optimal pre-stretch condition exists to achieve this maximum deflection.

Sustainable manufacturing: Membrane inflation is a key to optimizing the efficiency of businesses that utilize blow moulding and thermoforming processes (in which a heated sheet of plastic is inflated into the shape of a Mold). Membrane (or pre-stretch) control can ensure that the wall thickness of the final product is uniform and reduce the amount of plastic that is wasted during production.

REFERENCES

1. Adkins J.E. and Rivlin R.S., 1952. Large elastic deformation of isotropic materials IX. *Philosophical Transactions of the Royal Society of London. Series A, Mathematical and Physical Sciences*, 244, pp.505-531.

2. Arruda E. and Boyce M.C., 1993. A three-dimensional constitutive model for the large stretch behavior of rubber elastic materials. *Journal of the Mechanics and Physics of Solids*, 41(2), pp.389-412.

3. Campbell J.D., 1956. On the theory of initially tensioned circular membranes subjected to uniform pressure. *Quarterly Journal of Mechanics and Applied Mathematics*, 9(1), pp.84-93.

4. Christensen R.M. and Feng W.W., 1986. Nonlinear analysis of the inflation of an initially flat, circular, elastic disk. *Journal of Rheology*, 30, pp.157-165.

5. DasGupta A. and Jayprakash K., 2009. Inflation dynamics of a circular membrane. *9th International conference on vibrational problems*, IIT Kharagpur, India.

6. Feng W.W. and Huang P., 1974. On the inflation problem of a plane nonlinear membrane. *Journal of Applied Mechanics*, 40, pp.9-12.

7. Feng W.W. and Huang P., 1975. On the general contact problem of an inflation nonlinear membrane. *Journal of Applied Mechanics*, 11, pp.437-442.

8. Feng W.W. and Yang W.H., 1973. On the contact problem of an inflated spherical nonlinear membrane. *Journal of Applied Mechanics*, 40, pp.209-214.

9. Foster H.O., 1967. Inflation of a plane circular membrane. *Journal of Engineering for Industry*, 89, pp.403-407.

10. Goncalves P.B., Soares R.M. and Pamplona D., 2009. Nonlinear vibrations of a radially circular hyperelastic membrane. *Journal of Sound and Vibration*, 327, pp.231-248.

11. Green A.E. and Adkins J.E., 1960. *Large Elastic Deformations and Non-Linear Continuum Mechanics*. Oxford, Oxford University Press.

12. Hart-Smith L.J. and Crisp J.D.C., 1967. Large elastic deformation of thin rubber membranes. *International Journal of Engineering Science*, 5, pp.7-24.

13. Jha A.K. and Inman D.J., 2004. Importance of geometric non-linearity and follower pressure load in the dynamic analysis of a gossamer structure. *Journal of Sound and Vibration*, 278(1), pp.207-231.

14. Khayat R.E., Derdorri A. and Garcia-Rjon A., 1992. Inflation of an elastic cylindrical membrane: Non-linear deformation and instability. *International Journal of Solids and Structures*, 29(1), pp.69-87.

15. Klingbeil W.W. and Shield R.T., 1964. Some numerical investigation on empirical strain energy functions in the large axisymmetric extension of rubber membranes. *Journal of Applied Mathematics and Physics*, 15, pp.608-629.

16. Mooney M., 1940. A theory of large elastic deformation. *Journal of Applied Physics*, 11, pp.582-592.

17. Nadler B., 2010. On the contact of spherical membrane enclosing a fluid with rigid parallel planes. *Journal of Nonlinear Mechanics*, 45(3), pp.294-300.

18. Patil, A. and DasGupta, A., 2013. Finite inflation of an initially stretched hyperelastic circular membrane. *European Journal of Mechanics - A/Solids*, 41, pp.28-36.

19. Pamplona D., Goncalves P.B. and Lopes S.R.X., 2006. Finite deformations of cylindrical membranes under internal pressure. *International Journal of Mechanical Sciences*, 48, pp.683-696.

20. Pamplona D., Goncalves P.B., Davidovich M. and Weber H.I., 2001. Finite axisymmetric deformations of an initially stressed fluid-filled cylindrical membrane. *International Journal of Solids and Structures*, 38, pp.2033-2047.

21. Pamplona D.C. and Bevilacqua L., 1992. Large deformation under axial force and moment loads of initially flat annular membranes. *Journal Non-Linear Mechanics*, 27(4), pp.639-650.

22. Pujara P. and Lardner T.J., 1978. Deformation of elastic membranes: effect of different constitutive relations. *Journal of Applied Mathematics and Physics*, 29, pp.315-327.

23. Rivlin R.S., 1948. Large elastic deformation of isotropic materials-Fundamental concepts. *Philosophical Transactions of the Royal Society of London. Series A, Mathematical and Physical Sciences*, 240, pp.459-490.

24. Sahu, S. and Roychowdhury, S., 2022. An anisotropic hyperelastic inflated toroidal membrane in lateral contact with two flat rigid plates. *Acta Mechanica Solida Sinica*, Vol. 35, pp. 1068-1081.

25. Selby J.C. and Shannon M.A., 2009. Inflation of a circular elastomeric membrane into horizontally semi-infinite liquid reservoir of finite vertical depth: Quasi-static deformation model. *International Journal of Engineering Science*, 47, pp.700-717.

26. Selvadurai A.P.S., 2006. Deflections of a rubber membrane. *Journal of the Mechanics and Physics of Solids*, 54, pp.1093-1119.

27. Taber L., 2004. *Nonlinear theory of elasticity-Application in biomechanics*. World Scientific Publications. Tielking J.T. and Feng W.W., 1974. The application of the minimum potential energy principle to nonlinear axisymmetric membrane problems. *Journal of Applied Mechanics*, 41, pp.491-496.

28. Verron E., Khayat R.E., Derdouri A. and Peseux B., 1999. Dynamic inflation of hyperelastic spherical membranes. *Journal of Rheology*, 43(5), pp.1083-1098.

29. Verron E., Marckmann G. and Peseux B., 2001. Dynamic inflation of non-linear elastic and viscoelastic rubber like membranes. *International Journal for Numerical Methods in Engineering*, 50(5), pp.1233-1251.

30. Wong F.S. and Shield R.T., 1969. Large plane deformations of thin elastic sheets of neo-Hookean material. *Journal of Applied Mathematics and Physics*, 20, pp.176-199.

31. Yang W.H. and Feng W.W., 1970. On axisymmetrical deformation of nonlinear membranes. *Journal of Applied Mechanics*, 37, pp.1002-1011.

32. Yu L.K. and Valanis K.C., 1970. The inflation of axially symmetric membranes by linearly varying hydrostatic pressure. *Transactions of the Society of Rheology*, 14(2), pp.159-183.

33. Yu L.K. and Valanis K.C., 1970. The inflation of axially symmetric membranes by linearly varying hydrostatic pressure. *Transactions of the Society of Rheology*, 14(2), pp.159-183.

APPENDICES

Appendix A: Explicit Expressions for F_1 and F_2

(The full symbolic expressions for the right-hand sides of the ODEs, as generated by Mathematica and transcribed into MATLAB.)

$$
\begin{aligned}
&F_1(u_1, u_2, u_4, x, p, \alpha, \zeta) \\
&\qquad = \Bigg(\pi x u_1^4 (u_2^2 + u_4^2)^6 \Bigg(1 \\
&\qquad /(u_1^5 (u_2^2 + u_4^2)^5) 4 u_2 u_4 \big(x^2 \\
&\qquad + u_1^2 (\alpha + \zeta u_2^6 + 3\zeta u_2^4 u_4^2 + 3\zeta u_2^2 u_4^4 + \zeta u_4^6) \big) \Big(6x^4 u_1 u_4 - 4x^5 u_2 u_4 \\
&\qquad + 2\alpha u_1^5 u_4 (u_2^2 + u_4^2)^2 + x u_1^4 u_2 (px - 4\alpha u_4)(u_2^2 + u_4^2)^2 \\
&\qquad - 2x^2 u_1^3 u_4 (-\alpha + (1 - 2\zeta) u_2^4 + 2\zeta u_2^6 + 2u_2^2 (1 - 2\zeta + 3\zeta u_2^2) u_4^2 \\
&\qquad + (1 - 2\zeta + 6\zeta u_2^2) u_4^4 + 2\zeta u_4^6) \Big) \\
&\qquad - \Big((2\alpha u_1^2 u_2)/x^2 + (6x^2 u_2)/(u_1^2 (u_2^2 + u_4^2)^2) \\
&\qquad - \big(u_1 (-2 + 2\alpha u_2^2 + p x u_4 - 2\alpha u_4^2) \big)/x \\
&\qquad + 2u_2 (-1 + 2\zeta - 2\zeta u_2^2 - 2\zeta u_4^2 + \alpha/(u_2^2 + u_4^2)^2) \\
&\qquad + \Big(2x^3 \big(-\alpha - (2u_2^2)/(u_2^2 + u_4^2)^2 - 1/(u_2^2 + u_4^2) \big) \Big) /u_1^3 \Big) \Big(\alpha u_1^2 \\
&\qquad + \big(x^4 (-u_2^2 + 3u_4^2) \big)/(u_1^2 (u_2^2 + u_4^2)^3) \\
&\qquad + x^2 \big(1 - 2\zeta + u_2^2 (2\zeta - \alpha/(u_2^2 + u_4^2)^3) \\
&\qquad + u_4^2 (6\zeta + (3\alpha)/(u_2^2 + u_4^2)^3) \big) \Big) \Bigg) \Bigg) \\
&\qquad / \Bigg(2 \Bigg(16\pi x^2 u_2^2 u_4^2 \big(x^3 + x u_1^2 (\alpha + \zeta (u_2^2 + u_4^2)^3) \big)^2 \\
&\qquad - \pi \Big(x^4 (u_2^2 + u_4^2) - \alpha u_1^4 (u_2^2 + u_4^2)^3 \\
&\qquad - x^2 u_4^2 (4x^2 + 3\alpha u_1^2 + 6\zeta u_1^2 (u_2^2 + u_4^2)^3) \\
&\qquad - x^2 u_1^2 \big((u_2^2 + u_4^2)^3 - 2\zeta (u_2^2 + u_4^2)^3 \\
&\qquad - u_2^2 (\alpha - 2\zeta (u_2^2 + u_4^2)^3) \big) \Big) \Big(-3x^4 u_2^2 + x^4 u_4^2 - \alpha u_1^4 (u_2^2 + u_4^2)^3 \\
&\qquad - 3x^2 u_1^2 u_2^2 (\alpha + 2\zeta (u_2^2 + u_4^2)^3) \\
&\qquad - x^2 u_1^2 \big((u_2^2 + u_4^2)^3 - 2\zeta (u_2^2 + u_4^2)^3 - u_4^2 (\alpha - 2\zeta (u_2^2 + u_4^2)^3) \big) \Big) \Bigg) \Bigg)
\end{aligned}
$$

$$
\begin{aligned}
&F_2(u_1, u_2, u_4, x, p, \alpha, \zeta) \\
&\quad = \Big(-4u_2u_4(2\alpha u_2^2 + 2\alpha u_4^2 + 3)x^9 + 6u_1u_4x^8 \\
&\quad - 4u_1^2u_2u_4(2\alpha\zeta u_2^8 + (2\zeta - 1)u_2^4 + 8\alpha\zeta u_4^6u_2^2 + 2\alpha^2u_2^2 + 2\alpha\zeta u_4^8 \\
&\quad + (12\alpha\zeta u_2^4 + 2\zeta - 1)u_4^4 + 2(4\alpha\zeta u_2^6 + (2\zeta - 1)u_2^2 + \alpha^2)u_4^2 \\
&\quad + 3\alpha)x^7 \\
&\quad - 8u_1^3u_4(2\zeta u_2^6 + (1 - 2\zeta)u_2^4 + 2(3\zeta u_2^2 - 2\zeta + 1)u_4^2u_2^2 + 2\zeta u_4^6 \\
&\quad + (6\zeta u_2^2 - 2\zeta + 1)u_4^4 - \alpha)x^6 \\
&\quad + u_1^4u_2(u_2^2 + u_4^2)(8\alpha u_4^3 - 3pxu_4^2 + 8(\alpha u_2^2 + 1)u_4 - 3pxu_2^2)x^5 \\
&\quad + 2u_1^5u_4\big(4\zeta^2u_2^{12} + 4\zeta(1 - 2\zeta)u_2^{10} + (1 - 2\zeta)^2u_2^8 - 4\alpha\zeta u_2^6 \\
&\quad + 4\alpha(\zeta - 1)u_2^4 \\
&\quad + 4\big(6\zeta^2u_2^8 + 5\zeta(1 - 2\zeta)u_2^6 + (1 - 2\zeta)^2u_2^4 - 3\alpha\zeta u_2^2 \\
&\quad + 2\alpha(\zeta - 1)\big)u_4^2u_2^2 + 4\zeta^2u_4^{12} + 4\zeta(6\zeta u_2^2 - 2\zeta + 1)u_4^{10} \\
&\quad + (60\zeta^2u_2^4 + 20\zeta(1 - 2\zeta)u_2^2 + (1 - 2\zeta)^2)u_4^8 \\
&\quad - 4(-20\zeta^2u_2^6 + 10\zeta(2\zeta - 1)u_2^4 - (1 - 2\zeta)^2u_2^2 + \alpha\zeta)u_4^6 \\
&\quad + \big(60\zeta^2u_2^8 + 40\zeta(1 - 2\zeta)u_2^6 + 6(1 - 2\zeta)^2u_2^4 - 12\alpha\zeta u_2^2 \\
&\quad + 4\alpha(\zeta - 1)\big)u_4^4 + \alpha^2\big)x^4 \\
&\quad + u_1^6u_2(u_2^2 + u_4^2)\Big(16\alpha\zeta u_4^9 - 6px\zeta u_4^8 \\
&\quad + 4(16\alpha\zeta u_2^2 + \alpha - 2\alpha\zeta + 2\zeta)u_4^7 - px(24\zeta u_2^2 - 2\zeta + 1)u_4^6 \\
&\quad + 12u_2^2(8\alpha\zeta u_2^2 + \alpha - 2\alpha\zeta + 2\zeta)u_4^5 - 3pxu_2^2(12\zeta u_2^2 - 2\zeta + 1)u_4^4 \\
&\quad + 4(16\alpha\zeta u_2^6 + (-6\zeta\alpha + 3\alpha + 6\zeta)u_2^4 + \alpha^2)u_4^3 \\
&\quad - 3px(8\zeta u_2^6 + (1 - 2\zeta)u_2^4 + \alpha)u_4^2 \\
&\quad + 4(4\alpha\zeta u_2^8 + (-2\zeta\alpha + \alpha + 2\zeta)u_2^6 + \alpha^2u_2^2 + 2\alpha)u_4 \\
&\quad - pxu_2^2(6\zeta u_2^6 + (1 - 2\zeta)u_2^4 + 3\alpha)\Big)x^3 \\
&\quad - \alpha u_1^8u_2(px - 4\alpha u_4)(u_2^2 + u_4^2)^4x - 2\alpha^2u_1^9u_4(u_2^2 + u_4^2)^4\Big) \\
&\quad /\big(6u_1x^9 \\
&\quad + 4u_1^3\big((2\zeta - 1)u_2^4 + 2(2\zeta - 1)u_4^2u_2^2 + (2\zeta - 1)u_4^4 + 3\alpha\big)x^7 \\
&\quad + 2u_1^5\big(-12\zeta^2u_2^{12} + 8\zeta(2\zeta - 1)u_2^{10} - (1 - 2\zeta)^2u_2^8 + 4\alpha(\zeta - 1)u_2^4 \\
&\quad - 4(60\zeta^2u_2^4 + 20\zeta(1 - 2\zeta)u_2^2 + (1 - 2\zeta)^2)u_4^6u_2^2 \\
&\quad - 4\big(18\zeta^2u_2^8 + 10\zeta(1 - 2\zeta)u_2^6 + (1 - 2\zeta)^2u_2^4 - 2\alpha(\zeta - 1)\big)u_4^2u_2^2 \\
&\quad - 12\zeta^2u_4^{12} - 8\zeta(9\zeta u_2^2 - 2\zeta + 1)u_4^{10} \\
&\quad - (180\zeta^2u_2^4 + 40\zeta(1 - 2\zeta)u_2^2 + (1 - 2\zeta)^2)u_4^8 \\
&\quad + 2\big(-90\zeta^2u_2^8 + 40\zeta(2\zeta - 1)u_2^6 - 3(1 - 2\zeta)^2u_2^4 + 2\alpha(\zeta - 1)\big)u_4^4 \\
&\quad + 3\alpha^2\big)x^5 \\
&\quad - 4\alpha u_1^7(u_2^2 + u_4^2)^2(4\zeta u_2^6 + (1 - 2\zeta)u_2^4 + 2(6\zeta u_2^2 - 2\zeta + 1)u_4^2u_2^2 \\
&\quad + 4\zeta u_4^6 + (12\zeta u_2^2 - 2\zeta + 1)u_4^4 + \alpha)x^3 - 2\alpha^2u_1^9(u_2^2 + u_4^2)^4x\big)
\end{aligned}
$$

CURRICULUM VITAE

Sunil Bishwakarma

Linkedin: Sunil Bishwakarma Email:sunil.bishwak@gmail.com
Mobile: +91-9044482067

SKILLS

- **Languages**: MATLAB
- **Tools**: SolidWorks, Ansys, Abaqus, NX Cad, AutoCAD, Fusion 360, MS Office (Word, Excel, PowerPoint)
- **Soft Skills**: Problem-Solving Skills, Team Player, Project Management, Adaptability

INTERNSHIP

- **TVS Sundram fasteners Ltd.** Sept 2022 - Dec 2022
  Intern
  - **About**: Worked in production department where different mechanical and automobile components are manufactured using CNC for Navistar, Inc which is an American holding company. Thus, I am familiar with product machining and its inspection as well as quality checking.

PROJECTS

- **Impact Energy Absorption Analysis of Ss304 Pu Foam–Al6061 Sandwich Panel by Using Abaqus.**
  Aug 2025 - Nov 2025
- **Fabrication And Characteristics of Aluminum Metal Matrix Composites for The Automobile Application.**
  Apr 2023 – Aug 2023
  • learnt about composites and their fabrication using powder metallurgy process.
  • Got an idea about different processes such as compaction and sintering along with metal powder handling process.
- **Design and Analysis of Fluid Flow and Aerodynamic Forces on NACA 4412 Airfoil Using CFD.**
  Jan 2020 – May 2020
  • Used CFD for the analysis of lift and drag on the airfoil.
  • Solved Navier–Stokes equations to evaluate lift and drag coefficients.
  • Analyzed mesh sensitivity and boundary conditions.

PUBLICATIONS

- **An Investigation on the Mechanical Properties of Graphene Nanocomposite. [CHAPTER]**
- **Mechanical Properties of Fiber Metal Laminate Hybrid Composite Materials. [CHAPTER]**
- **Investigation of induction hardening on heat-treated EN8 steel by alternately timed quenching process. [Article]**

CERTIFICATES

- **Design Practice- Indian Institute of Technology, Kanpur**
  Roll No: NPTEL25ME16S534101746
- **Automation in Manufacturing- Indian Institute of Technology, Guwahati.**
  http://nptel.ac.in/noc Roll No: NPTEL21ME120S33340468
- **Wind Energy- DTU - Technical University of Denmark.**
  link

ACHIEVEMENTS

- **Fully Funded Scholarship from Government of India, Indian Embassy (ICCR)**: August 2024
  Pursuing M-tech under Sushma Swaraj Silver Jubilee Scholarship Scheme

EDUCATION

- **Delhi Technological University** Delhi, India
  Master of Technology – Computer Aided Analysis and Design; ***CGPA:9.0/10*** *2024-Present*
- **Vel Tech Rangarajan Dr. Sagunthala R&D Institute of Science and Technology** Chennai, India
  Bachelor of Technology - Mechanical Engineering; ***CGPA: 9.24/10*** *2019-2023*
- **Golden Gate International Higher Secondary School** Kathmandu, Nepal
  Intermediate; ***GPA: 3.29/4*** *2017 – 2018*
- **Little Angels Higher Secondary School** Nawalparasi, Nepal
  Matriculation; ***GPA: 3.5/4*** *2015 - 2016*